NASA CR 66923

EXPLORATORY ELECTROMAGNETIC THRUSTER RESEARCH

PHASE III

by

A. C. Ducati and R. G. Jahn

prepared for

NATIONAL AERONAUTICS AND SPACE ADMINISTRATION

Contract NAS 1-9297

Plasmadyne
a division of GEOTEL, INC.
Santa Ana, California

NASA CR 66923

Report FR-020-9297

EXPLORATORY ELECTROMAGNETIC THRUSTER RESEARCH
PHASE III

by

A. C. Ducati and R. G. Jahn

prepared for

NATIONAL AERONAUTICS AND SPACE ADMINISTRATION
Langley Research Center
Hampton, Virginia 23365

Contract NAS 1-9297

February 1970

Plasmadyne
a division of GEOTEL, INC.
Santa Ana, California

FOREWORD

This is the report on work carried out during the period of 23 June 1969 to 23 December 1969 by Plasmadyne, a division of Geotel, Inc., on Phase III of "Exploratory Electromagnetic Thruster Research," Contract NAS 1-9297, originating in the Plasma Physics Division, Langley Research Center, Hampton, Virginia, under the direction of James M. Hoell.

Adriano C. Ducati was the Principal Investigator in charge of the work. Robert G. Jahn collaborated as a consultant, Rene' Bregozzo participated in the conduction of the experiments, and Willis Stoner contributed to the preparation of this report.

TABLE OF CONTENTS

LIST OF ILLUSTRATIONS

LIST OF ILLUSTRATIONS (Cont.)

LIST OF SYMBOLS

b	dimension defined in Figure 28
c	damping coefficient
C	capacitance
D	diameter of the steel ball
e	coefficient of restitution
f	frequency of pulses in a series - also a steady force used for calibration and damping force
F	thrust force - also continuous force equivalent in impulse to a series of pulses
g	acceleration of gravity
h	maximum height to which the ball is raised
I	moment of inertia about the pivot axis
ΔI	moment of inertia of weights added to the platform for calibration
I_{sp}	specific impulse
I_t	total impulse applied
J	electrical current
k	torsional spring constant of the platform
KE	kinetic energy
$\ell_{effective}$	effective pendulum length
L	inductance
L_C	self inductance of capacitors
n	number of pulses in a series - also number of sections in a pulse generating network
P_J	power during a pulse
P_S	primary source power
Q	heat
r	radius at which thrust is applied - also radius of a swinging steel ball
r_a	anode radius
r_c	cathode radius
R	radius at which the displacement is measured

R_L	resistance of inductors
s	distance
t	time measured from the beginning of a pulse
t_J	pulse length
t_o	time at the end of a pulse
t_q	inception time
T	natural torsional period of the platform - also pulse duration, duration of a series of pulses, and temperature
T_s	natural swinging period of the platform
V	voltage - also velocity of the steel ball
V_h	horizontal component of V
V_o	initial network voltage
x	linear displacement at radius (r)
x'	linear displacement at radius (R)
Z	impedance
Z_a	arc impedance
Z_L	characteristic line impedance
α	angle of inclination
α_c	specific mass of the power conditioning system (kilograms per joule)
α_p	specific mass of the primary power source (kilograms per joule)
δ	duty cycle fraction
η	efficiency of thruster or power transfer efficiency
θ	angular displacement of the platform
θ_o	θ at the end of a pulse
θ_{max}	maximum value of θ
μ	magnetic permeability
τ	two-way transmission time
Φ	phase angle
ω	angular velocity
ω_o	initial angular velocity

1.0 INTRODUCTION

This report describes work performed for evaluating the performance of MPD arc jets operating in the quasi-steady mode. This type of operation is obtained by running the thruster at a high power level for a pulse period of the order of one millisecond; a period which is short enough to avoid the major problems associated with continuous high power operation, but long enough that steady state operating conditions appear to be attained during most of the pulse duration. The system consists of a thruster, a pulse generating network, a method for starting the arc, and a method for providing the proper flow of propellant during the pulse. Strong interest has recently developed in this type of thruster because the possibility exists of realizing the performance advantages of high power operation without the need for a space power system capable of continuous operation at high power levels, and without encountering the heating problems and life problems associated with continuous high power operation. Performance at high power levels is believed to be more attractive because self-field effects become predominant at high arc current levels, and because viscous losses and heat transfer losses become a smaller fraction of the total power input at high power density.

In addition, operation in short pulses may permit more meaningful test results to be obtained. One of the problems in evaluating the performance of continuously running MPD thrusters has been that the contribution to thrust caused by the entrainment and acceleration of ambient gas has not yet been accurately determined. With a pulsed thruster, it is possible to thoroughly evacuate the test chamber before initiating the pulse so that actual space conditions are more closely simulated. Furthermore, there is the possibility of making certain probe measurements in the plume that would be impractical with steady operation. These include velocities obtained by the double probe method, and the use of probes that would overheat in a continuous plume. There are, of course, also measurements (such as the propellant flow rate) that are more difficult to make with pulsed operation. The quasi-steady work is expected to supplement rather than replace results obtained from continuously operating thrusters in improving our understanding of MPD thruster performance.

Work on the development of a propellant feed system has focused on the use of solid and liquid propellants. These materials can be attractive because of their good storability; and, with some solid materials, it may be feasible to use rods or sleeves of propellant as electrodes or insulating components that are continuously renewed by feeding to offset the rate of erosion. Such an arrangement is expected to result in long thruster life. Another possibility is that waste materials or discardable spacecraft hardware can be utilized for propellant if satisfactory performance can be demonstrated. It is believed that thrusters operating in the self-field regime give performance that is less critical to the choice of propellant than would be the case with a purely thermal acceleration device.

The work reported here is concerned primarily with setting up an initial engine system and with developing techniques for measuring performance with quasi-steady operation.

2.0 ENGINE DESIGN

2.1 Initial Considerations

The two major considerations in implementation of repetitive-pulse laboratory operation are the preparation and transmission of the desired current pulse train, and the properly synchronized injection of suitable propellant mass pulses into the accelerator. The choice of technique for accomplishment of either of these depends heavily on just those temporal characteristics of the pulse train -- its rise time, pulse length, duty cycle, etc. -- whose effects on thruster performance it is desired to assess, and hence some intuition and versatility are needed at the outset. Broad constraints on the pulse characteristics can be imposed on the basis of certain experience with single-pulse experiments, and of reasonable limitations on the overall power system. For example, from single-pulse experiments over the range of 4000 to 140,000 A it is found:[1]

a. For any given pulse amplitude, J, there is an inception time, t_q, before proper quasi-steady operation ensues, given roughly by t_q (sec) $\approx$ 1/2 J (amp). To insure that quasi-steady operation prevails over most of the pulse, one might thus require a pulse length at least one order of magnitude longer, say $t_J \geq 5/J$.

b. Once quasi-steady operation is achieved, the accelerator consumes power at a rate $P_J = V J = J^2 Z$ where the accelerator impedance, Z, is very nearly constant at a value between 0.005 and 0.010 ohm, depending mainly on the accelerator size.

c. Pulse rise times need not be shorter than the quasi-steady inception time, t_q.

To these may be added certain constraints on behalf of the overall power system, for example:

d. The mean power consumption is limited by the particular primary source, P_S:

$$\delta P_J < \eta P_S$$

where δ is the duty cycle fraction and η the transfer efficiency.

e. The mass of the power conditioning system, which will reside mainly in the electrical storage units needed for pulse formation, should not exceed that of the primary power source. The former probably scales nearly linearly with the requisite pulse energy, $J^2 Z t_J$, at a few hundredths of a kilogram

per joule, and the latter with mean power at some hundredths of a kilogram per watt.

Manipulation of such relations leads to various duty cycle -- pulse length -- arc current domains reasonable for exploratory quasi-steady thruster operation at given mean power levels, such as shown in Figure 1.

Over most of the pulse length-duty cycle domain indicated by such calculations, the most convenient and versatile power source for laboratory experiments is the lumped-element transmission line or so-called "LC ladder network," composed of a succession of n identical sections, each consisting of a shunt capacitance, C_1, and a series inductance, L_1, (Figure 2).[2, 3] One end of this line is connected to the accelerator via a series inductance of about one-half the single section value, and the other end to a charging supply capable of returning the line voltage to the desired value, V_o, at the desired repetiton rate. Values of the line parameters, n, L_1, C_1, and V_o, are based on optimization of several interlocked considerations:

1. The characteristic impedance of the line, Z_L, should be close to that of the quasi-steady discharge, Z_a, to maximize the electrical energy transfer and to avoid ringing or overdamping of the pulse waveform:

$$Z_L = \sqrt{\frac{L_1}{C_1}} = \sqrt{\frac{L}{C}} \approx Z_a \tag{1}$$

where L and C denote the total inductance and capacitance deployed in the line.

2. The two-way transmission time of the line must equate to the desired pulse length:

$$\tau = 2n\sqrt{L_1 C_1} = 2\sqrt{LC} = 2 Z_L C = t_J \tag{2}$$

3. The capacitors must withstand the charging voltage necessary to drive the desired pulse current through the accelerator:

$$V_o = J_a (Z_a + Z_L) \tag{3}$$

4. The self-inductance of the individual capacitors and their terminal connections must be substantially smaller than the single section inductance if the configuration is to discharge as a line:

$$L_C < L_1 \tag{4}$$

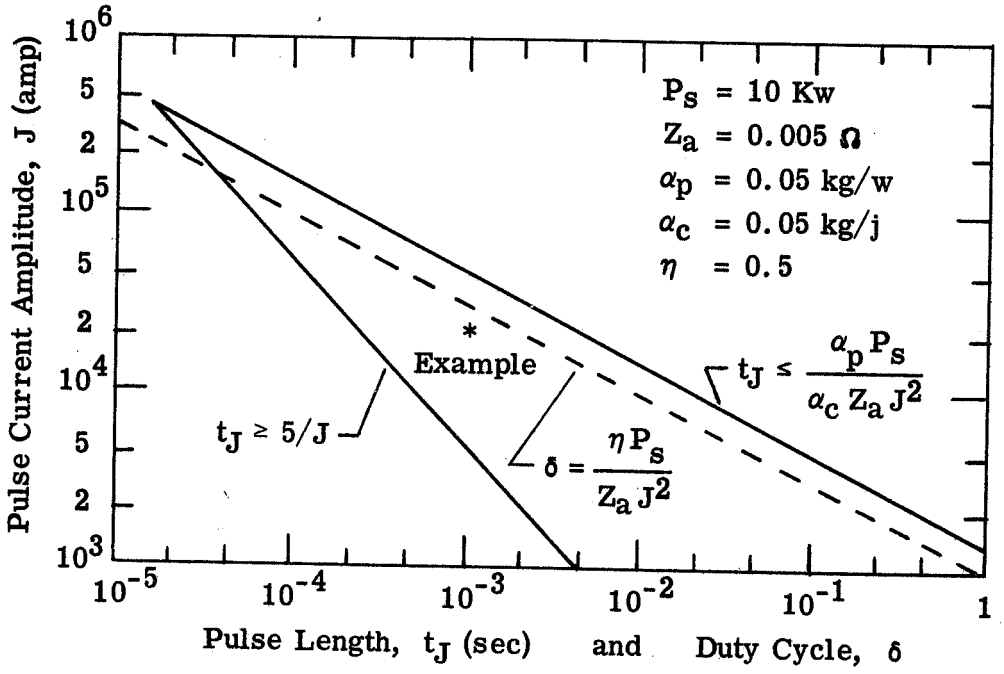

Figure 1. Typical Domain of Current Pulse Profiles of Interest to Quasi-Steady Propulsion

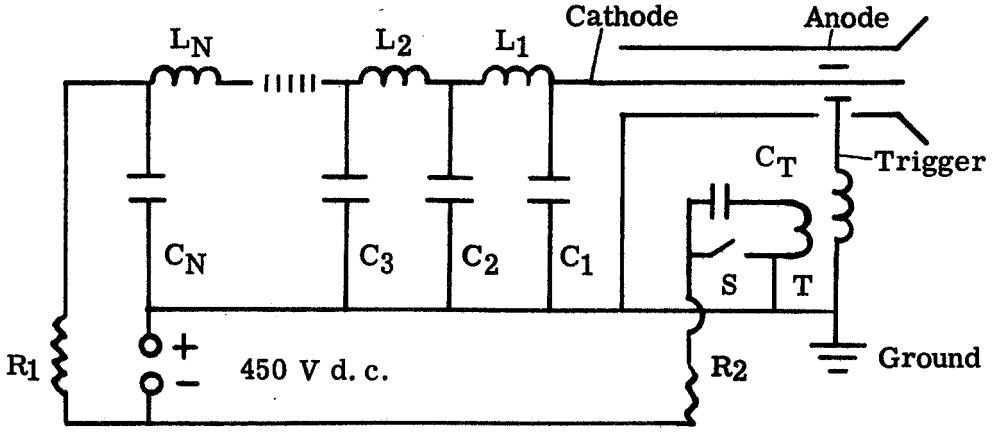

Figure 2. Electrical Schematic of Quasi-Steady Experiment

5. The resistance of the inductors must be very small or the pulse will suffer an "L/R droop":

$$L_1/R_L \ll t_J \tag{5}$$

6. The number of sections must be sufficient to keep the pulse ripple below a tolerable level. This is an involved function of all line parameters, but typically dictates at least five, and preferably ten or more sections; say

$$5 < n < 20 \tag{6}$$

7. The physical size and mass of the line assembly must be tolerable in the particular experimental application. This factor becomes particularly important when the power source is to be mounted inside a vacuum chamber or on a thrust stand.

It is difficult to generalize the results of the multi-dimensional trade-off implicit in the above list over the broad domain of possible operation outlined in Figure 1, but certain characteristics of the facility can be defined. Because the accelerator impedance is relatively fixed in the milli-ohm range, the available pulse length is essentially proportional to the total capacitance deployed (2), and the total inductance is then fixed if the line is to be matched to the accelerator (1). Note that if this match prevails, the total charge stored in the line can be equated to that passing through the accelerator in one pulse, and the total stored energy to that delivered to the accelerator:

$$CV_o = J\,t_J \tag{7}$$

$$\frac{1}{2}\,CV_o^2 = J\,V_a\,t_J = J^2\,Z_a\,t_J \tag{8}$$

so that the line voltage is fixed by the desired pulse current:

$$V_o = 2\,Z_a\,J \tag{9}$$

To illustrate with a particular example, consider the operation of a 0.005 ohm accelerator with 0.001 sec pulses of 20,000 A, a condition fairly central to the $J - t_J$ domain of Figure 1. Relation (2) immediately demands a total capacitance of 100,000 μfd, and (1) calls for a total inductance of 2.5×10^{-6} H. Relation (9) indicates the line should be charged to 200 V.

This tendency to large capacitance and relatively low voltage is characteristic of the quasi-steady accelerator application because of its inherently low impedance and the time scale of interest. Even with a 20-section line, the required single-section capacitance in the above example would be 5000 μfd, which raises nontrivial questions of the mass,

size, convenience and cost of the complete configuration. On the other hand, the single-section inductors, 1.25×10^{-7} H each, can be readily provided from a few turns of very heavy conductor.

If one of the above factors precludes assembly of the requisite large total capacitance, the $J - t_J$ regime of interest can be reached only with a mismatched line, i. e., one whose characteristic impedance is larger than the accelerator load. Various options then can be considered:

a. Couple the line to the accelerator via a transformer to achieve the desired match. For the pulse parameters considered here this would probably require a unit whose mass, bulk and cost are comparable with that of the total capacitance needed for a directly matched line.

b. Add a series resistor to increase the impedance of the load to that of the line. Clearly, a major portion of the line energy will then be dissipated in the resistor, but voltage and current reversal will be avoided.

c. "Crowbar" the line with a switch and dummy load at the appropriate time in the discharge cycle. Less energy is lost by this technique, but the electrical system becomes more complex.

d. Accept the damped ringdown pattern of current and voltage reversals.

While one of these techniques may suffice for a particular type of laboratory experiment, it seems imperative that any space propulsion system operate in a closely matched configuration.

2.2 Capacitors

The development of serviceable pulsed plasma propulsion systems has been hindered in the past by a lack of systematic attention to the design and construction of electrical storage units optimized for this particular application. The requirements on low specific mass, low inductance and internal resistance, very high pulse number capability, vacuum operation, etc., are largely at odds with classical capacitor concepts and construction, and attempts to adapt conventional units to this purpose have typically frustrated the preparation of an attractive propulsion package. * Of the little research that has been attempted in this direction, most has concerned the reduction of capacitor inductance to

*The exception would be those applications where specific mass is not a controlling factor, such as certain very low power satellite adjustment tasks, where pulsed plasma systems have performed well.[4]

permit faster rise times, pulse-shaping, and improved energy transfer to low impedance discharge loads for laboratory experiments in the microsecond-pulse regime.[2, 5]

To provide the millisecond pulses indicated for quasi-steady operation, two further specifications now must be added to the list of desirable capacitor attributes: very large total capacity, and low voltage operation. The construction and deployment of energy storage units possessing all such desirable properties becomes a major problem even for laboratory experiments in this realm; for space propulsion systems it may well be the controlling factor. Investigation of this problem merits at least comparable attention with study of the accelerators themselves.

Capacitors may be broadly classed into four categories, reflecting the nature of the insulation between their charge-storing plates; (a) vacuum or gas gap; (b) liquid dielectric; (c) solid or composite dielectric; (d) chemical or electrolytic. Of these, the first two are rarely used in discharge work because of their large plate spacings and correspondingly low energy storage densities. The third class is most commonly employed, usually with oil-impregnated kraft paper or mylar as the dielectric, separating aluminum foil electrodes. Such units, if properly configured, can have low internal inductance and resistance, and can be designed to withstand charging voltages up to 10^5. Even at these high voltages, however, their specific mass and volume are uncomfortably large, as evidenced by the monumental capacitor arrays commonly found at most experimental plasma facilities.

Electrolytic capacitors provide their own dielectric layer by electrochemical oxidation of the surface of one electrode (anode), adjacent to an electrolytic substance (cathode). This layer is so thin, $\sim 10^{-7}$ m, that the capacitance per unit mass and volume can be many orders of magnitude greater than the paper dielectric units, but also because of its thinness, the layer cannot withstand potentials of more than about 500 V. Even at these voltages, however, the specific mass and specific volume of electrolytic capacitors are smaller than the paper units by at least one order of magnitude, and, as discussed above, low voltage storage is inherently better suited for the quasi-steady accelerator application. That is, the optimum charging voltage and accelerator terminal voltage are commensurate for the electrolytics; for the paper capacitors they are not. A paper-capacitor network charged to 10^4 to 10^5 V is badly mismatched to its accelerator; if charged to only a few hundred volts, its specific mass is completely intolerable.

Notice that the size advantage of electrolytic capacitors becomes more marked in cases where it is desired to operate at voltages that are lower than the 500-volt practical limit. As voltage is reduced, the energy stored by electrolytic capacitors tends to reduce directly with the voltage, instead of with the square of the voltage, as is the case with paper capacitors. This is because with reduced voltage electrolytic capacitors operate with a thinner insulating layer and therefore have a higher capacitance. This is not possible when the minimum commercially available dielectric thickness is reached.

Electrolytic capacitors have several fundamental disadvantages which have heretofore discouraged this type of application. First, they are inherently asymmetric in their polarity. Any significant reversal of their electrode voltage dissipates the insulating oxide layer, and the circuit is shorted. Second, even when properly polarized, they allow higher leakage currents than the paper units. Third, because one electrode is an electrolyte, their internal resistance tends to be comparatively high. Finally, at least in electronic applications, their reliability and life are normally inferior to paper capacitors.

Despite their characteristic disadvantages, it seems reasonable to explore the possible use of electrolytic capacitors in the quasi-steady accelerator application, first because of their desirable high capacity, low voltage properties, and second because there appears to have been no systematic attempt to improve this class of capacitor for this particular type of service. As will be seen, the immediate benefit of this choice is a far simpler, smaller, and less expensive laboratory installation.

2.3 Propellant Feed

The second logistical complication inherent in a quasi-steady propulsion system is the preparation and injection of suitably tailored pulses of propellant mass, properly synchronized with the driving current pulse train. In conventional short-pulse accelerators it is well-established that such synchronization, and the details of the ambient propellant distribution in the accelerator at discharge initiation, are extremely important to the overall thrust efficiency.[6, 7] In such inherently unsteady devices where "snowplow" acceleration processes function on a microsecond time scale, the slightest mismatch in spatial and temporal distribution of propellant with the particular acceleration pattern can have serious effects on the propellant utilization and dynamic efficiencies. The corresponding sophistication required of gas injection systems for short-pulse accelerators has never been completely attained.

Operation in the quasi-steady mode should considerably relax these demands on the precision of propellant injection. The longer pulse durations allow more slack in the initiation and termination of the mass pulse without substantial detriment to the utilization efficiency, and the details of the ambient spatial distribution at breakdown are largely inconsequential. In the same spirit as the current pattern stabilization criteria (Section 2.1-a), such transient effects should be absorbed in the bulk of the quasi-steady operation. In addition to the relaxed rise-time requirements, an external valve system now must operate many times less over a given total impulse operation.

Nonetheless there remain nontrivial requirements for provision of intermittent mass flow pulses, constant over the quasi-steady pulse duration at a rate appropriate to the arc current and amplitude, and synchronized with its waveform. For single-pulse experiments, well-tailored mass profiles have been provided by a shock tube injector

technique,[1] but this is clearly inapplicable to multiple pulse operation. For this, one must return to high speed mechanical valves, or undertake development of more sophisticated fluid dynamic or plasmadynamic flow modulation techniques.

Since this program is focusing on the use of solid and liquid propellants, it is of interest to explore the possibility that the arc chamber can be designed to vaporize material at a suitable rate to provide the desired propellant flow during a pulse. Normally, conventional plasma jets run with four sources of propellant. The material that is fed into the arc chamber to act as a propellant is augmented by vapor from the electrodes, vapor from insulating material, and entrained ambient gas. It may be attractive to eliminate the usual gaseous propellants and to operate entirely on materials that are vaporized in the arc chamber. Low power vacuum arcs have been developed for thruster application in both short pulse[4] and steady modes,[8, 9] and the ability of high power, steady MPD arcs to function in this manner is well-known.[10]

The use of a solid or liquid propellant can be attractive because materials with good storability can be selected and because of the possibility of suitable materials becoming available as waste materials or discardable hardware. In addition, if the propellant can double as an electrode or an insulator in the arc chamber, continuous renewal of this element may lead to long thruster life. On the other hand, any material that offers the above advantages must have a low vapor pressure at normal temperatures in order to avoid excessive vaporization between pulses.

The problem of synchronizing the propellant feed with the arc current pulse is clearly less difficult if the propellant is a solid that can be used as an electrode. Local vaporization appears to start very rapidly when the arc is initiated, and to stop equally fast at the end of the pulse. However, if the propellant takes the form of an insulating material or a liquid that must be fed into the arc chamber, direct heating by the arc is more difficult to achieve. The situation must be avoided that requires heating of a significant portion of solid material before propellant vaporization can start as this would result in a serious lag between the arc pulse and the propellant pulse. Figure 3 shows one arrangement that has been used for locating the insulating material so that it will be directly heated by the arc.

Tests have been initiated using solid materials for the propellant. The use of liquids appears to be more difficult and is still being studied. It may be feasible to feed a liquid through a porous tungsten electrode in a manner that results in vaporization of the liquid as soon as the arc is initiated. This would be easier to accomplish with a conducting material such as mercury or an alkali metal, since the arc could strike directly on the liquid, and would tend to migrate to parts of the electrode with filled pores. However, it may also be feasible to use a nonconducting liquid such as vacuum oil. Notice that the

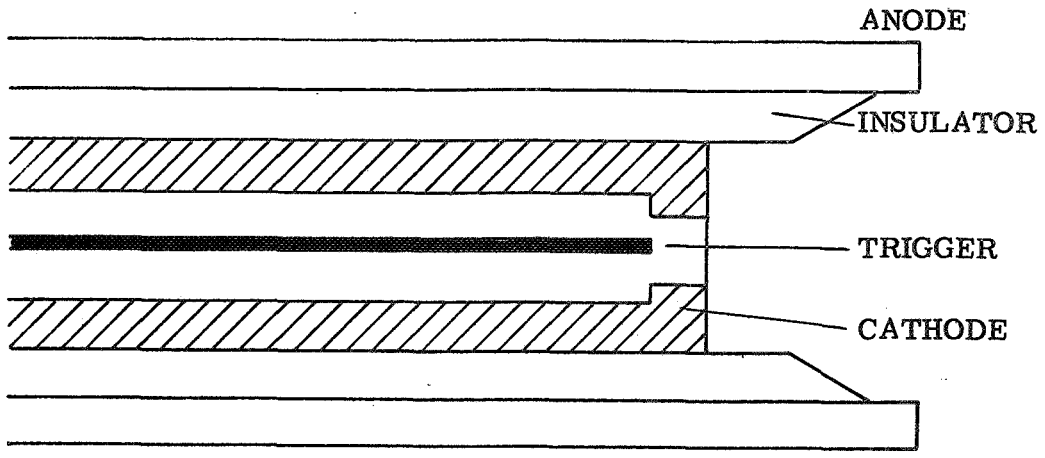

Figure 3. Cross Section of Vacuum Arc Accelerator Head

propellant expended per pulse is no more than one or two milligrams, and it is not anticipated that much of the porous material will be emptied during a pulse. A critical aspect of the problem is that the pores should be filled with liquid at the beginning of the pulse to provide evaporative cooling for all parts of the porous tungsten when the arc is initiated. However, the liquid should not flow through the pores and drip from the electrode between pulses. Unfortunately, a random pore geometry with uniform wetting properties would result in flow through the pores if enough pressure were applied to cause filling of the pores. Possible solutions include control of the feed pressure so that the flow of propellant is only slightly more than the evaporation rate, and the development of porous electrodes with constrictions in the pores near the electrode surface so that surface tension effects would prevent further flow of liquid. The latter arrangement would require a non-wetting combination. Experimental work with liquid propellants is being delayed until a method can be found to avoid contamination of the test chamber and vacuum system by mercury and alkali metal propellants.

During this program tests have been initiated for studying the erosion of electrodes of various materials and geometries when exposed to a long series of pulses. Figure 4 shows five cathodes of various materials which had identical dimensions initially and were tested for identical duty cycles. The much more rapid erosion rate evident for the aluminum cathode suggests that a wide range of vaporization rates may be readily obtainable by varying the electrode design. Some of the material is usually discharged as particles as well as vapor, as evidenced by visible sparks in the plume. This effect is, of course, detrimental to performance since the particles are ejected at velocities that are much lower than the average. It is not known at present what fraction of the mass flow comes off in the form of solid particles.

Figure 5 shows five anodes of various materials which had identical dimensions initially and were tested for identical duty cycles. These electrodes were used in a

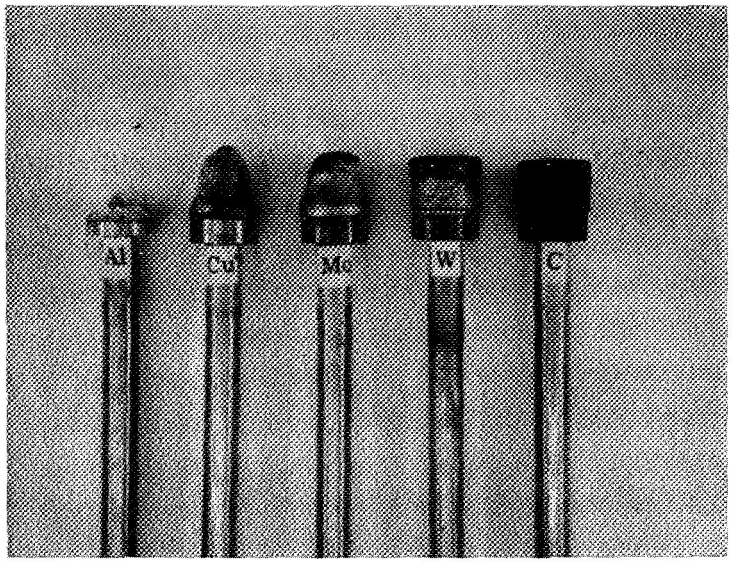

Figure 4. Comparative Erosion Tests of Five Cathodes

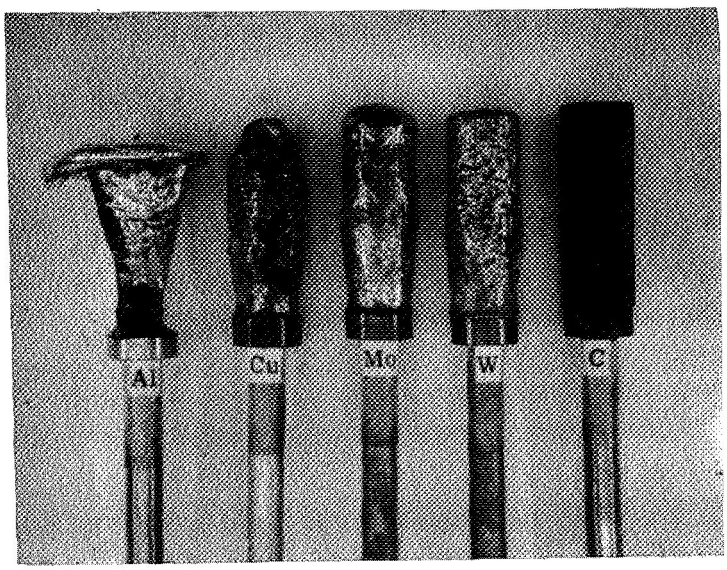

Figure 5. Comparative Erosion Tests of Five Anodes
(Used in Reverse Polarity Configurations)

thruster with reverse polarity. Although the electrodes exhibit rather extensive thermal distortion, the net loss of material is surprisingly low (much less than was noted for cathodes of similar design). This is contrary to expectations because the anode fall region loss is considerably larger than that for the cathode, and it was anticipated that an increase rate of vaporization would follow. Presumably, the anode arc foot is enough more diffuse to more than offset the increased heating rate. Another unexpected result was the peculiar deformations observed in the metal anodes. The low temperature materials appear to mushroom at their ends, while the higher temperature materials seem to bulge in the center. Since electromagnetic forces would be in the direction to pinch or stretch the electrode rather than to cause it to bulge, it is assumed that the deformation is caused by thermal stresses which arise during repeated pulses. An exception is the portion of the self-field thrust force due to higher gas pressure at the end of the center electrode, but this force can be no more than a few pounds. Rapid heating of the outer surface of the cylindrical electrode would result in compression at the outside and tension at the center, and could conceivably result in cracks opening up in the central region after repeated cycles. Studies are under way to establish the nature of the deformations in greater detail. It would be interesting to section some of the electrodes in the bulging regions to see if internal cracks are evident. Much of the electrode surface appears to have been molten, and it is possible that the liquid material tends to collect at a favored location. However, no explanation has been suggested for upstream migration of the materials.

An explanation is also lacking so far for the strikingly different behavior of the aluminum anode. Aluminum has a thermal diffusivity in between that for copper and molybdenum; however, it does have the lowest melting point of the materials used, the lowest density, and the highest value of the heat of vaporization (with the exception of graphite). Transient heat transfer studies are needed to determine if aluminum would be expected to develop a thicker layer of molten metal during a pulse than the other materials.

The nearly undisturbed condition of the graphite anode is particularly noteworthy. Graphite has two unique characteristics; it sublimes, and it has a heat of vaporization that is about ten times as large as that for tungsten. Both properties appear to be advantageous. While the graphite anode was in use, no sparks were observed in the plume. This suggests that many of the particles observed may originate as liquid droplets carried away from electrodes that have molten surfaces.

In considering which materials are preferable for use as propellants to be vaporized by the arc, it is useful to compare the energy needed to vaporize the material to the kinetic energy in the jet. The ratio of these quantities has been plotted as a function of specific impulse for a number of propellants in Figure 6. The heat required for vaporization was calculated starting at 20°C or at the saturated liquid condition, whichever is cooler. To avoid the need for a large amount of cooling, it would be desirable to choose a propellant that requires an amount of heat nearly equal to the normal electrode heat loss.

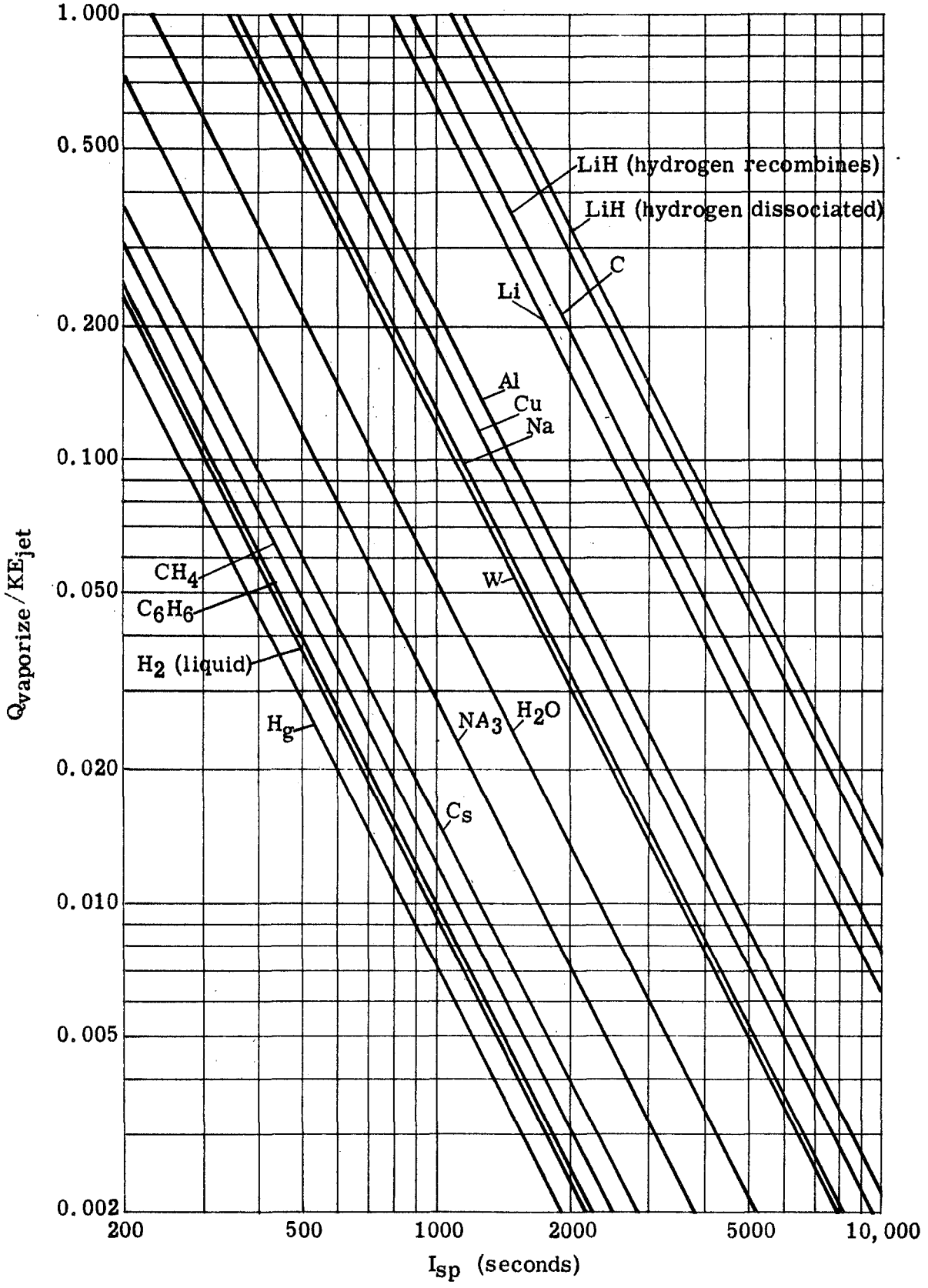

Figure 6. Energy Fraction Needed to Vaporize the Propellant

From this standpoint, propellants such as carbon, lithium or lithium hydride appear most suitable if attractive values of specific impulse are to be obtained. However, other materials may be usable if adequate electrode cooling can be provided. Heat transfer studies are again needed to evaluate the amount of electrode cooling required with different designs and duty cycles.

Another property of propellants which has been considered is the energy required for ionization of the vaporized material. Some degree of ionization is required for an MPD thruster to operate effectively. Figure 7 shows the ideal energy for full single ionization expressed as a ratio of the jet kinetic energy and plotted as a function of specific impulse. Notice that the energy required for hydrogen is an order of magnitude higher than for the other propellants shown. Since satisfactory MPD thruster performance is obtainable with hydrogen, it is concluded that the energy needed for ionization of other propellants does not represent a serious loss.

As an initial step in the evaluation of electrode heat transfer, calculations have been made of the temperature in a cylindrical graphite electrode with a constant uniform flow of heat suddenly applied at the end of the rod. A heat flow rate of 788 kw/cm^2 was assumed. This corresponds to one megawatt applied to a rod one-half inch in diameter. It is believed that heating rates this large will be experienced when the 0.2 farad capacitor bank is put in use. To simplify the analysis, material properties were assumed constant. Calculated temperature profiles based on Chart 41 of Reference 11 are shown in Figure 8. It is seen that, with this high heat flow rate, the surface temperature would be high enough for vaporization to start within 36 microseconds, leaving the major portion of the pulse for operation with a flow of vapor supplied. However, at the start of vaporization, the temperature 0.1 mm below the surface would be essentially undisturbed. This very high initial temperature gradient would, of course, be accompanied by extremely severe thermal stresses, and would undoubtedly result in shattering of the graphite surface. It appears necessary to preheat the electrodes. This will be obtained automatically when the thruster is operated in repetitive pulses. If this were done, vaporization would start almost immediately, and cooling would be provided primarily by ablation.

2.4 Initial Performance Measurements

The reasoning outlined in the preceding sections led to a series of exploratory experiments involving a self-field vacuum MPD accelerator driven in a repetitive quasi-steady mode by an electrolytic capacitor line. The schematic of the system is the same as shown in Figure 2. The accelerator is mounted on the end wall of a large fiberglass vacuum tank 20 feet long by 8 feet in diameter, capable of evacuation to less than 10^{-6} torr.[12] The arc head itself is a coaxial assembly of an annular copper anode, a teflon insulator, an annular copper cathode, and a conical-tipped tungsten trigger electrode

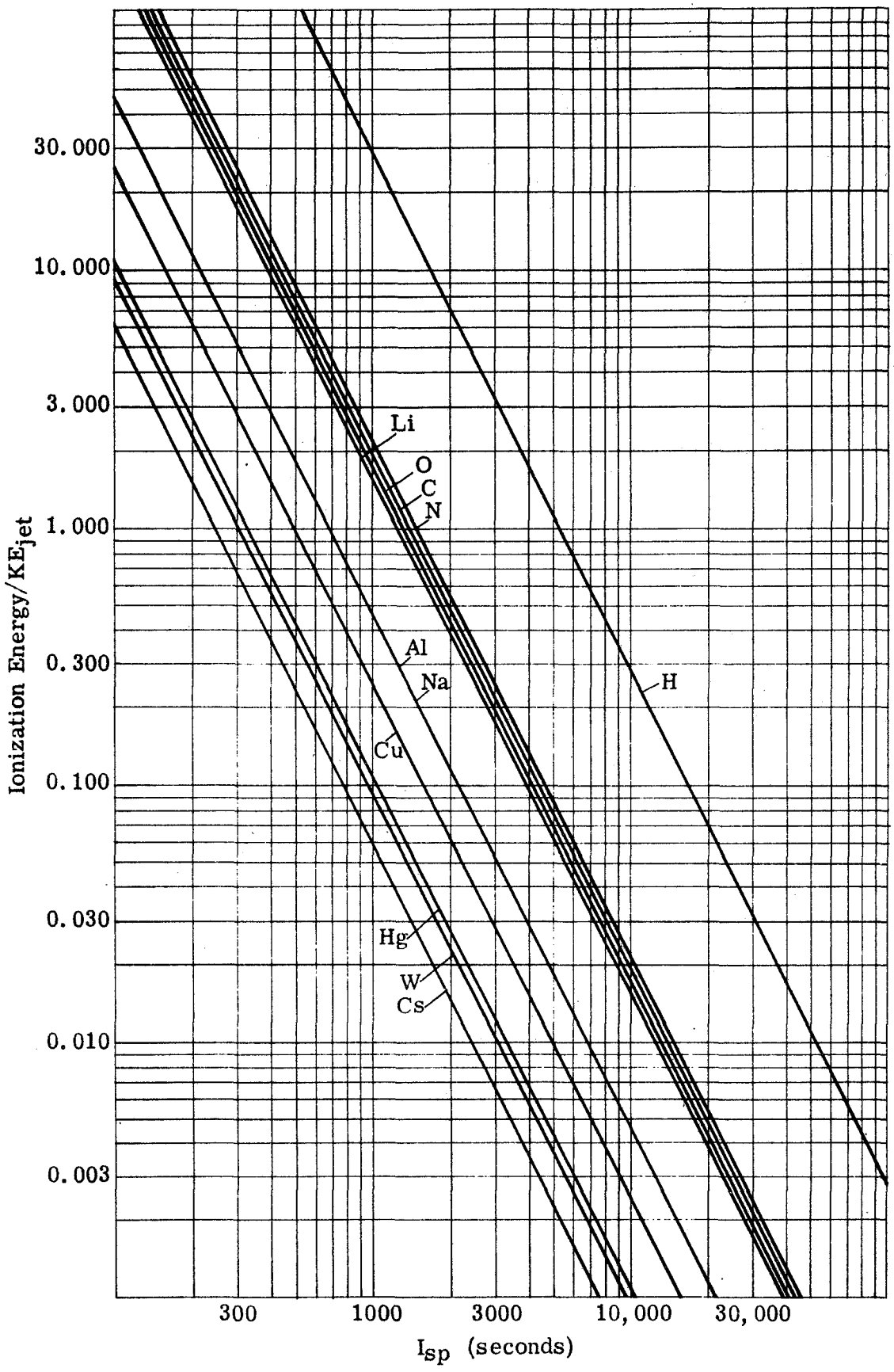

Figure 7. Ideal Energy for Full Single Ionization
(Expressed as a Ratio of Jet Kinetic Energy)

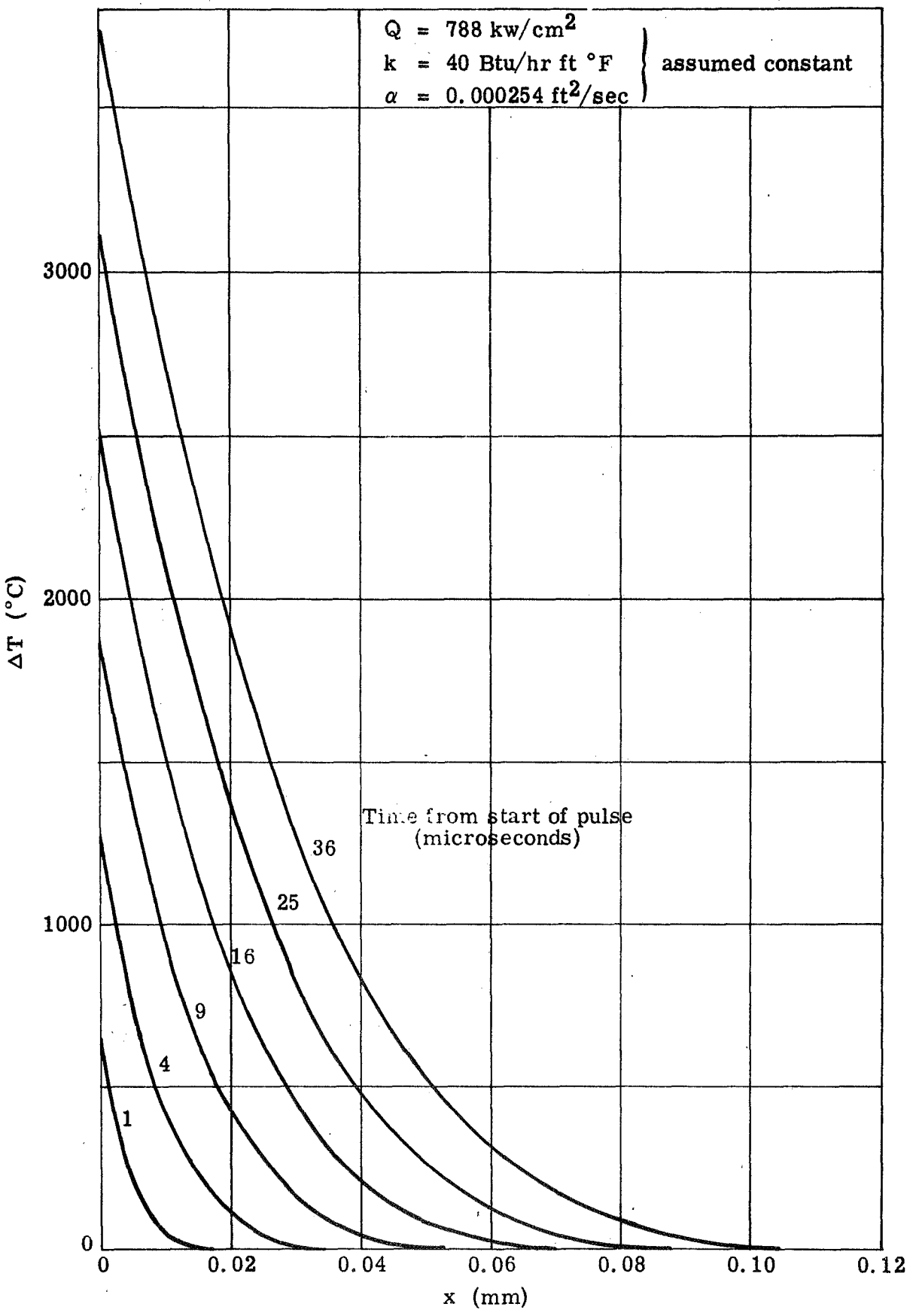

Figure 8. Calculated Temperature Variation for Step Function Heat Flow Into the End of a Cylindrical Graphite Rod

arranged as shown in Figure 3. The trigger electrode is energized by a 20 kV signal from the pulse transformer circuit which initiates a small discharge whose function is to provide sufficient ionization for the main gap to break down at the low line voltage.

The main pulse line for the initial test was constructed from twenty electrolytic capacitors, rated 1000 μfd x 450 V each (Sprague Model 6626), connected by suitable inductors which are selected by trial and error after initial estimate. In one configuration, for example, these inductors are simply three-turn coils, 3 inches in diameter, of heavy insulated copper wire 1/8 x 1/4 inch cross section, comprising about 5×10^{-7} H each. When these are used at every station of the line, its nominal impedance is about 0.022 ohm, and its pulse length about 900 μsec.

In actual operation, the internal resistance of the capacitors, and to a lesser extent the inductors, is sufficient to distort the pulse substantially from the desired rectangular shape (Figure 9a). This tendency may be remedied empirically by lowering the interstation inductance of the units farthest from the load. For example, Figure 9b shows the pulse shape obtained when the first eight sections of the line contain the three-loop inductors mentioned above and the last twelve are connected directly with 2-inch lengths of 1/2 x 1/32 inch brass strip. This particular pulse has a tolerably fast rise time of about 100 μsec, and a useful flat portion of nearly 500 μsec before beginning its slow decay. The line configuration producing this pulse, shown in the photograph of Figure 10, is that used for most of the initial experiments.

From the simultaneous arc current and voltage traces shown in Figure 9b we can already deduce certain properties of the discharge. First, when the current is steady, the voltage is steady, an excellent indication that the current pattern in the accelerator is stationary and that the device has attained quasi-steady operation. The terminal impedance of the accelerator during this period, $85 \text{ V} \div 16,000 \text{ A} \approx 0.005\ \Omega$, is in the typical MPD range. Note that despite the mismatch between this value and the nominal line impedance, the current does not reverse, but damps to zero monatonically. Furthermore, with the moderate values of inductance used in this test, the voltage does not reverse, but retains a positive "set" of some 35 volts after the current has subsided. It is not clear whether these effects derive from the unipolarity of the electrolytic capacitors, or from the characteristics of the vacuum arc, or both. Subsequent tests with increased inductance to lengthen the pulse do show some voltage reversal in the tail-off region (Figure 11). The study of this effect is complicated by the tendency of the electrolytic capacitors to prevent current reversals. The analysis will be presented in a later report.

Repetitive operation of the system described above is limited by the capacity of the charging circuit, and by resistive heating of the line inductors. The available rectifier bank is capable of returning the capacitor line to 450 volts in one second, so that repetitive operation can be triggered at rates up to once per second. Since the pulse power

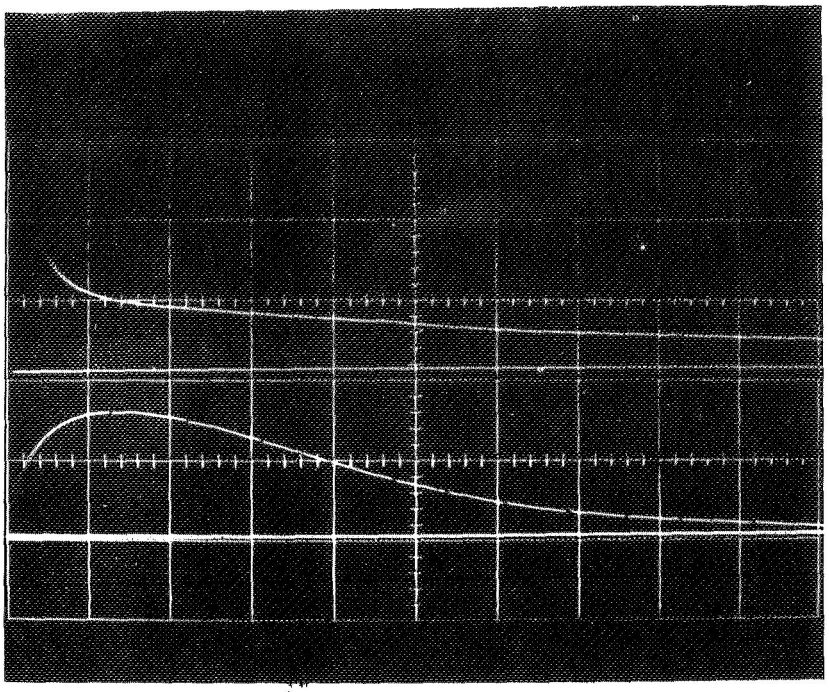

Figure 9a. Voltage and Current Profiles of Pulse from Nominal 0.022 Ω x 900 μsec Line, Distorted by Internal Resistance

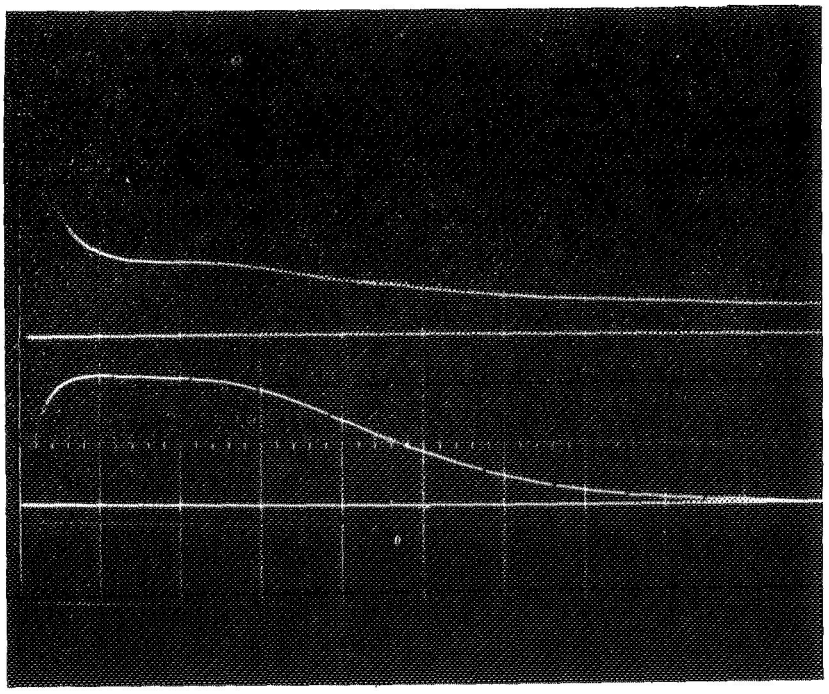

Figure 9b. Voltage and Current Profiles of Pulse from Line Modified to Balance Internal Resistance

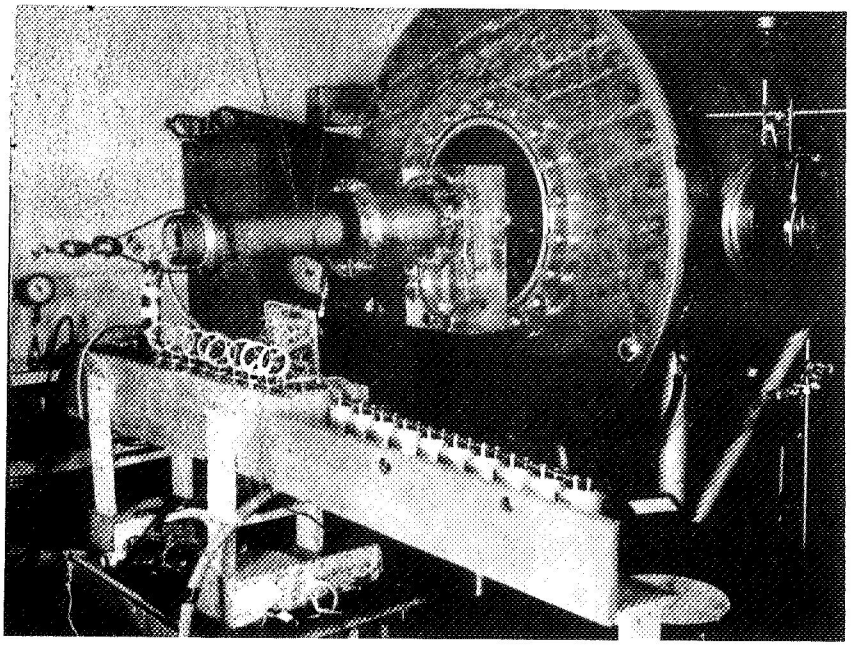

Figure 10. Photograph of Modified Capacitor Line Assembly

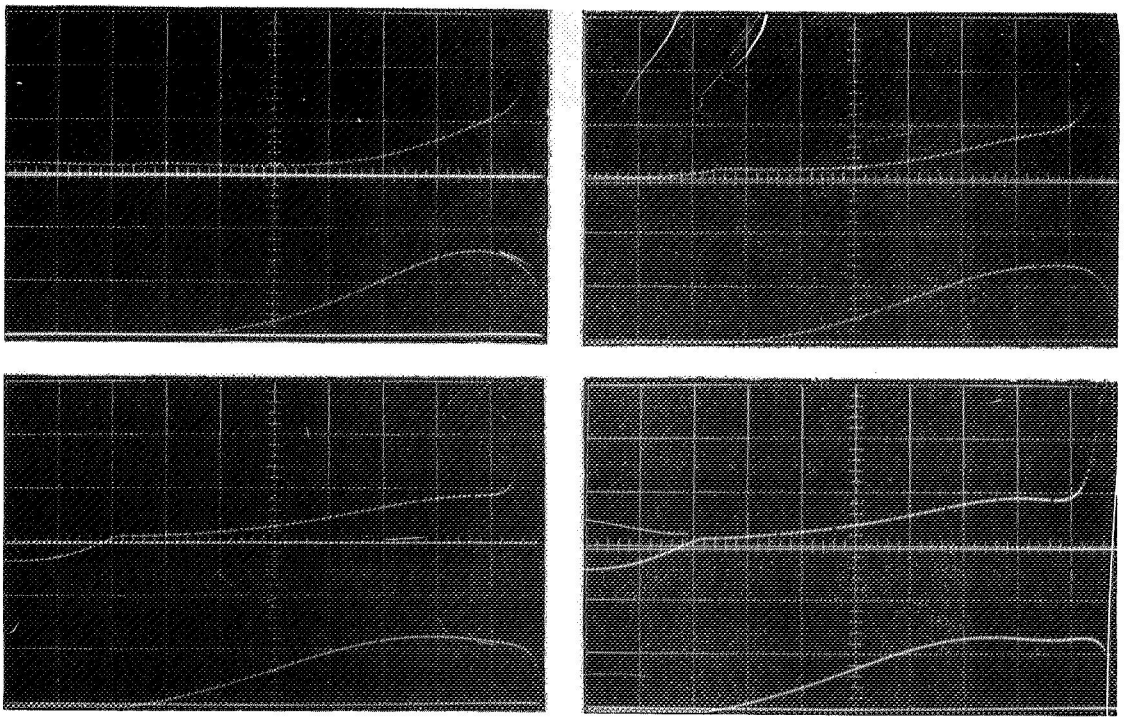

Figure 11. Gradual Modification of Voltage and Current Profiles Obtained With Coils of Reduced Resistance

is about 1.4 mw for one msec, this corresponds to operation at a mean power level of about 1.4 kw. Figure 12 shows an overlay of current waveform for ten successive pulses, which indicates the reproducibility of circuit and arc operation.

After the accelerator had been fired 500 times in this manner, it was dissembled, and its components weighed with the following results:

Net mass loss of anode (copper)	0.33 gm
Net mass loss of cathode (copper)	0.77 gm
Net mass loss of insulator (teflon)	1.30 gm
Net mass loss of trigger electrode (tungsten)	----
Total mass loss	2.45 gm
Average mass loss per pulse	~ 0.005 gm
Average rate of mass loss during pulse	~ 5.0 gm/sec

Figure 13 is a photograph of the thruster components after dissembly. Note the asymmetries in the erosion patterns on the cathode and insulator.

The computed value of the average rate of mass loss during a current pulse may not accurately reflect the true quasi-steady level of mass utilization by the accelerator because of its observed tendency to eject large solid particles sporadically. Figure 14 is a photograph of the luminous exhaust pattern downstream of the anode orifice which shows trajectories of several heavy particles sprayed from the accelerator.

At present, work on the pulse generating network is concentrating on configurations with reduced resistive loss. An effort is being made to retain the desired pulse shape while reducing resistive heating without introducing a ringing condition that could be harmful to the capacitors. The experimental work is being done using the thruster arc to load the circuit so that the behavior of the circuit with the actual arc impedance variation is determined. A large range of inductance coils have been constructed to permit the circuit characteristics to be changed experimentally. Figure 15 shows a family of coils that can be connected to the network with inductance varying from 0.2 to 4.0 microhenrys. In addition, a rail and slide arrangement has been devised (Figure 16) to permit a continuous adjustment of the inductance of each section of the network. A different type of circuit behavior may be obtained by deliberately choosing an arrangement of coils that produces large values for the mutual inductances. Figure 17 shows a coil constructed for this purpose. The large coil can be nested around a row of capacitors with each capacitor connecting to a different tap on the coil. The effective result is a series of coils with the mutual inductances essentially equal to the self inductance of each coil. Figure 11 shows variations in the current and voltage profiles obtained by changing the

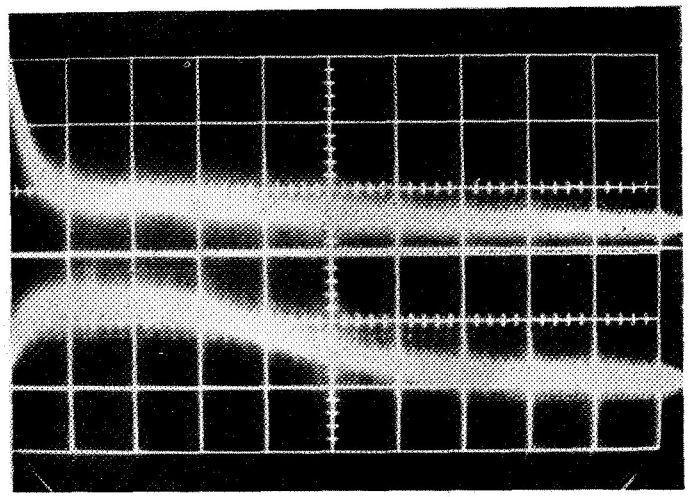

Figure 12. Ten-Pulse Overlay of Current Profile During Repetitive Operation

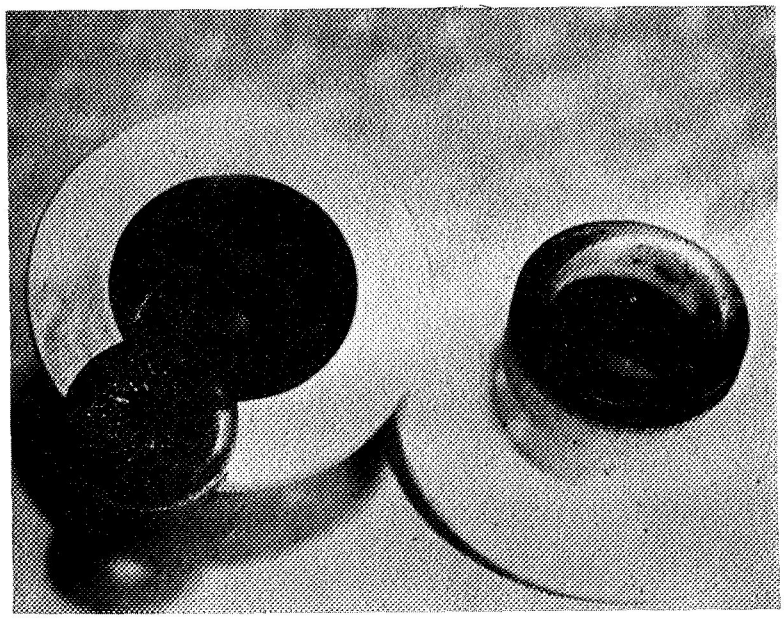

Figure 13. Photograph of Accelerator Components After 500 Pulses

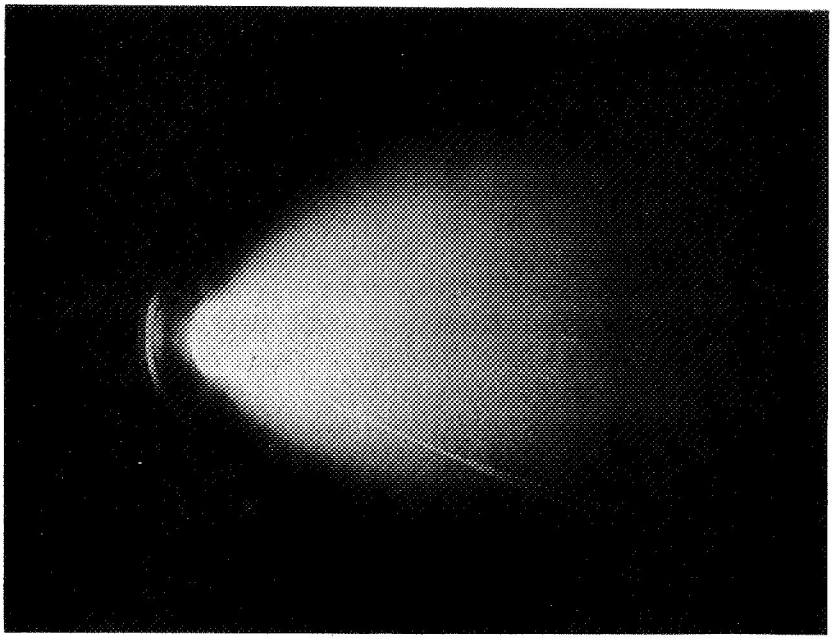

Figure 14. Exhaust of Quasi-Steady Vacuum Arc

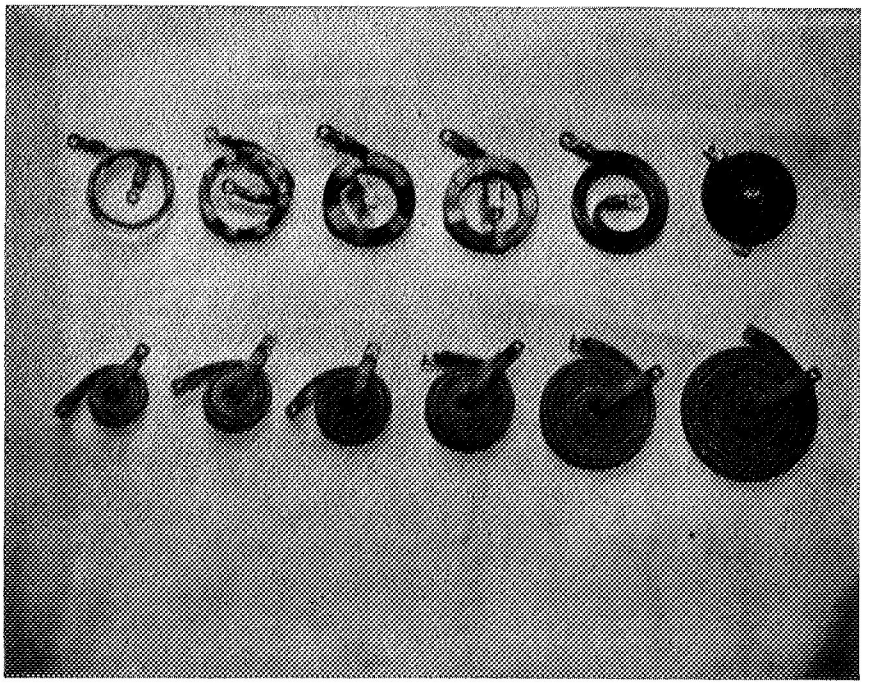

Figure 15. Family of Coils of Varying Inductance Used for the Experimental Development of the Pulse Generating Network

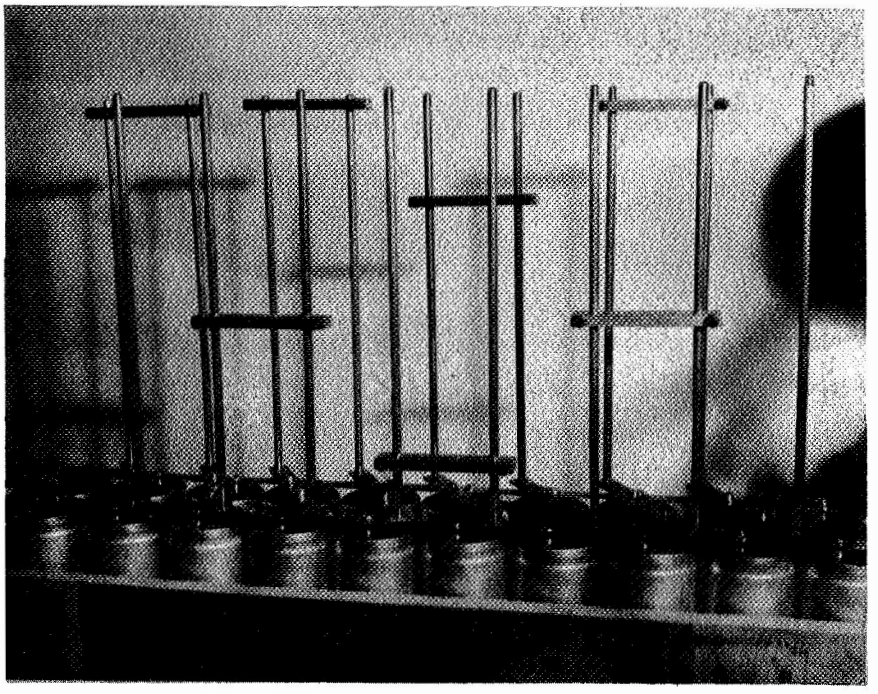

Figure 16. Rail and Slide Arrangement for Varying the Inductance of Sections of the Pulse Generating Network

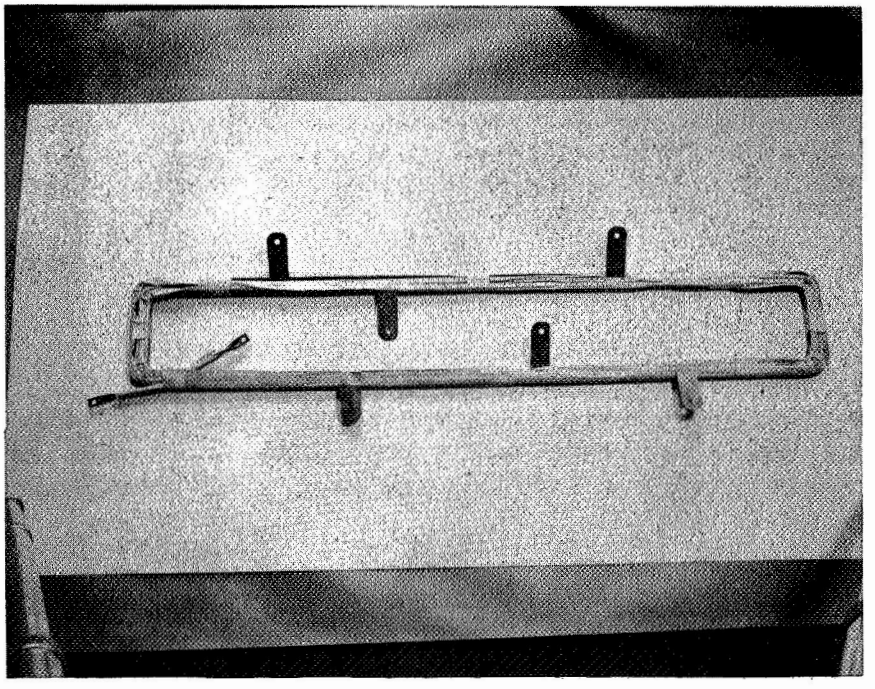

Figure 17. Coil Series Designed for Large Mutual Inductance

network parameters. The final trace pictured shows a region of nearly constant current lasting for one millisecond.

To obtain an indication of the exhaust velocity produced by the accelerator, a pair of electrostatic double probes, each biased by the circuit sketched in Figure 18, are placed at the far end of the vacuum tank at distances of 6.00 and 7.22 meters from the anode orifice. Figure 19 shows several of the probes installed in the test chamber while Figure 20 shows a close-up of the active end of one of the instruments. The probes can be moved in and out to give readings at any desired radius. The theory and operation of such probes are described in detail elsewhere;[13] briefly, when overrun by the burst of exhaust plasma, each probe circuit passes a signal proportional to the positive ion current to the more negative probe element. These ion current signatures bear characteristic features which can be identified on both probe circuits with separation times indicative of the prevailing plasma velocity. In this manner it is determined that the portion of the plasma accelerated during the quasi-steady portion of the pulse propagates down the tank centerline at about 15,000 m/sec. No attempt has yet been made to survey other portions of the exhaust plume, or to carry out a parametric survey of exhaust velocity as a function of arc parameters.

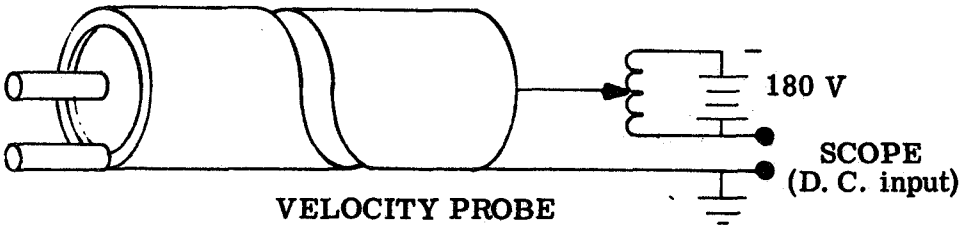

Figure 18. Velocity Probe Circuit

In addition to indicating that the accelerator is operating in an interesting range of specific impulse, this observed speed, combined with the admittedly questionable mass flow rate computed above, corresponds to a pulse thrust of about 75 newtons. For comparison, the classical self-field MPD relation[14]

$$F = \frac{\mu J^2}{4\pi}\left[\ln\left(\frac{r_a}{r_c}\right) + \frac{3}{4}\right]$$

predicts, for $J = 16,000$ A and $r_a/r_c = 2$, a thrust of about 37 newtons. The exhaust beam power corresponding to the measured values is about 0.56 mw, which would indicate a thrust efficiency of some 40 percent.

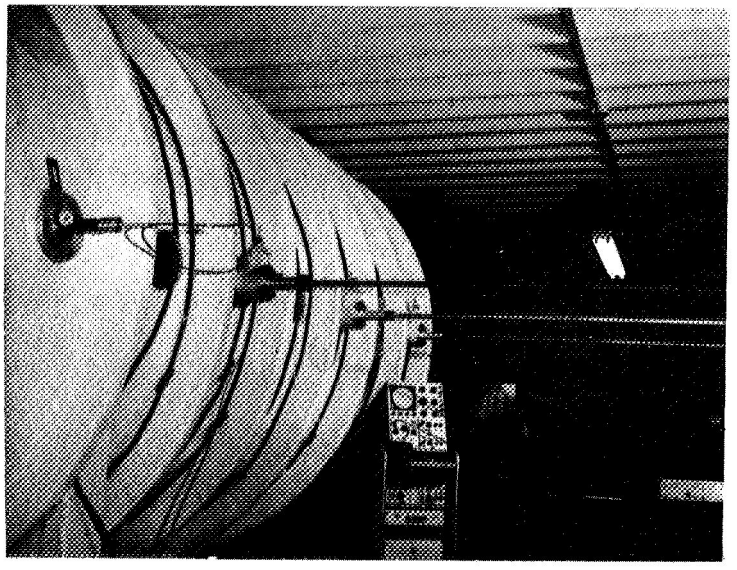

Figure 19. Velocity Probes Installed in the Test Chamber

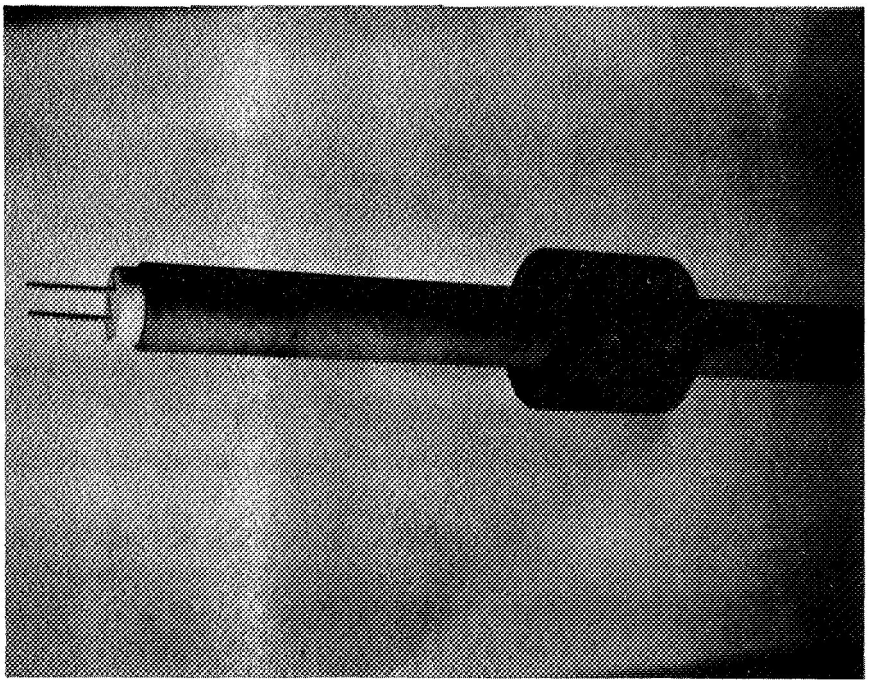

Figure 20. Electrode End of an Electrostatic Double Probe

In testing quasi-steady thrusters which use vaporized materials from the arc chamber for propellant, it is necessary to make frequent inspections of the electrodes and insulators, and to weigh these parts to determine erosion patterns and propellant consumption rates. In a conventional vacuum system this would require hours of pumpdown time because it would be necessary to release the vacuum in the chamber following each test in order to remove the thruster. However, the insulated tank used for these tests has a system for removing the thruster without releasing the vacuum in the chamber. The thruster is mounted on the end of a probe which can be inserted through a valved port in the chamber wall. An "O" ring seal in the port prevents leakage after the valve is opened. Figure 21 shows the valved port with the probe in place. A cable and winch is used to withdraw the probe against the force due to atmospheric pressure.

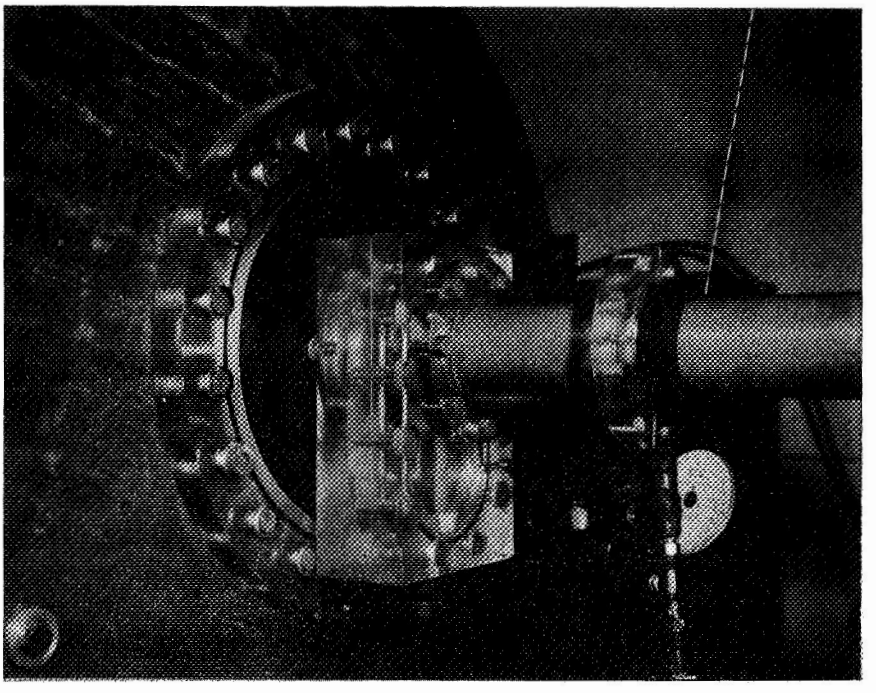

Figure 21. Valved Port for Introduction and Removal of the Thruster

3.0 DEVELOPMENT OF TESTING METHODS

3.1 The Measurement of Thrust

An evaluation has been made of several methods of measuring the impulse produced during a pulse, and some experiments have been conducted using a preliminary version of a torsional ballistic pendulum. As a result of this work, it has been concluded that the torsional ballistic pendulum is most suitable for the immediate needs of the program. Some of the analysis involved is presented in the pages that follow.

Although measurements giving the shape of the thrust pulses would be useful, there are some difficulties associated with obtaining good accuracy in the measurement of instantaneous thrust with plasma jets of this type. Rather than to undertake the development of such a thrust stand at this time, it appears preferable to conduct tests using a simple torsional type ballistic pendulum to accurately measure the total impulse produced by a series of pulses. This will permit overall performance figures for quasi-steady plasma accelerators to be available within a relatively short time period. A thrust plate is not considered satisfactory for this application because of uncertainties due to rapid spreading of the jet and circulation patterns stirred up in the test chamber. Accordingly, it is planned to mount the thruster with related equipment and connecting leads directly on the thrust stand. An experimental system of this type has been constructed, and tests are being conducted to establish requirements for the final design.

3.2 Difficulties Associated with Measurement of the Pulse Shape

A commonly used and very successful technique for measuring short thrust pulses involves the use of a solid state load cell directly coupled to the thruster to form a light rigid system. This type of load cell has an exceptionally high spring constant, and if the thruster can be kept light and the connecting structure rigid, high natural frequencies are possible. However, a number of problems would have to be solved in applying this technique to the type of thruster being considered.

1. Very high currents must be supplied momentarily to the thruster (20,000 amps in a typical case). This means that if the thruster alone were mounted on the load cell, heavy connecting leads would be required. These leads would have their own set of natural frequencies and would generally be subject to strong electromagnetic interaction forces. On the other hand, if the power conditioning system were mounted with the thruster as a unit, the added weight would reduce the primary natural frequency, and the natural frequencies of many components would be added to the system.

2. The expected pulse duration period of one millisecond is short enough to require special circuitry. As an example, consider the use of a Bytrex Model JP-500 load cell which has a capacity of 500 pounds and a spring constant of about 500,000 pounds per inch. This unit could conceivably be derated to operate with a 10-pound thrust load and still provide an adequate output signal. With a total engine system weighing 120 pounds attached to this load cell, the natural frequency would be about 202 cycles per second, while with a 12-pound thruster alone the natural frequency would increase to about 638 cycles per second. In both cases, the natural frequency is too low to permit direct measurements to be made. Circuitry is on the market for correcting signals of this type to allow for the natural frequency and damping characteristics of the structure in the thrust stand. Successful use has been made of this equipment in cases where the desired frequency response is an order of magnitude higher than structural natural frequencies. However, a certain amount of skill is required in adjusting the circuitry to match actual system characteristics, and the task of designing and adjusting the equipment becomes more difficult as the number of critical vibratory modes is increased.

3. The presence of a strong current pulse can result in a serious electromagnetic interference problem, particularly when weak signals are involved as is the case when a load cell is derated in order to make use of a unit with a high natural frequency. The arc must be open on the nozzle side, and clearly cannot be completely shielded. It is also difficult to provide a completely coaxial lead system all the way to the electrodes, and the load cell must be located close to the thruster to permit the design of a rigid structure. Exceptionally good shielding would therefore be required for the load cell and its leads.

4. Ambient vibrations are normally a problem whenever rapid response is required in measuring small thrust forces. The problem is increased by the presence of reciprocating vacuum pumps in the vicinity of the test chamber, and by the large mass of the experimental engine system. It is anticipated that a large seismic mass mounted inside the test chamber on a soft suspension system might be required to eliminate this type of signal error.

3.3 A Torsional Ballistic Pendulum

This type of instrument consists of a rotating platform suspended by a vertical wire at its pivot axis. Total impulse is determined by measuring the maximum rotary

displacement following an application of thrust to the platform in the tangential direction. The device appears to be well-suited for measuring the impulse associated with a series of pulses produced by quasi-steady plasma thrusters. The rotating platform can carry a large weight without much reduction in sensitivity, and so the instrument can be designed with the complete power conditioning system mounted on the platform with the thruster. This is an important advantage because the current flow to the platform may be reduced to that needed for recharging the condensers, and relatively small leads can be used. Exceptionally high sensitivity can be obtained by keeping the torsional spring constant of the supporting wire low. Auxiliary equipment will include a system for measuring the rotary displacement of the platform, an electromagnetic damper with near-critical damping which can be energized to stop the movement between readings, carefully designed flexible electrical leads to supply power and control signals to the platform, and an enclosure to protect the platform from aerodynamic disturbances. Ballistic pendulums are normally used to measure a single brief impulse applied with the platform initially at rest rather than a series of pulses distributed over a short time period. Some discussion is therefore in order regarding how the instrument would be used. For the case with a single impulse applied, the angular displacement of the platform can be related to the total impulse applied by equating the initial kinetic energy in the platform to the final energy stored in the torsion wire. We first find the initial angular velocity of the platform from momentum considerations:

$$r I_t = I \omega_o, \qquad \omega_o = \frac{I_t r}{I}$$

Then, equating energies,

$$\frac{1}{2} I \omega_o^2 = \frac{1}{2} k \theta_{max}^2$$

$$\frac{1}{2} I \left(\frac{I_t r}{I}\right)^2 = \frac{1}{2} k \theta_{max}^2$$

solving for the sensitivity,

$$\frac{\theta_{max}}{I_t} = \frac{r}{\sqrt{Ik}} \tag{10}$$

This relation shows that sensitivity can be increased by increasing the radius at which the thrust acts, by decreasing the moment of inertia of the platform, or by reducing the torsional spring constant of the system.

If a series of pulses are applied, a somewhat different response occurs which depends on the duration of the series. Oscilloscope traces of the current and voltage suggest that the performance is nearly identical for all of the pulses in a series.

If the pulses are uniform and closely spaced, a good approximation may be obtained by representing the series with a continuously applied thrust having the same total impulse and the same duration. The equation of motion for this model is,

$$Fr - k\theta = I \frac{d^2\theta}{dt^2}$$

which corresponds to simple harmonic motion of period

$$T = 2\pi\sqrt{\frac{I}{k}} \tag{11}$$

The phase, amplitude and displacement of the oscillations depend on the initial conditions and the magnitude of the applied thrust force (F). If the platform is initially at rest and time is measured from the first application of thrust, the solution becomes,

$$\theta = \frac{Fr}{k}\left[1 - \cos\left(\sqrt{\frac{k}{I}}\,t\right)\right] = \frac{Fr}{k}\left[1 - \cos\left(2\pi\frac{t}{T}\right)\right]$$

At the end of the pulse (time t_o)

$$\theta_o = \frac{Fr}{k}\left[1 - \cos\left(2\pi\frac{t_o}{T}\right)\right]$$

and

$$\left(\frac{d\theta}{dt}\right)_o = \frac{2\pi Fr}{Tk}\sin\left(2\pi\frac{t_o}{T}\right)$$

These last two quantities are the initial conditions for the remaining motion of the platform as it coasts to the maximum displacement condition with $F = 0$. The solution for this part of the motion is a sine wave centered about zero with a phase shift, and takes the form,

$$\theta = \theta_{max}\cos\left(2\pi\frac{t}{T} + \Phi\right)$$

$$\frac{d\theta}{dt} = -\theta_{max}\frac{2\pi}{T}\sin\left(2\pi\frac{t}{T} + \Phi\right)$$

Substituting the initial conditions,

$$\frac{Fr}{k}\left[1 - \cos\left(2\pi\frac{t_o}{T}\right)\right] = \theta_{max}\cos\left(2\pi\frac{t_o}{T} + \Phi\right)$$

$$\frac{2\pi Fr}{Tk}\sin\left(2\pi\frac{t_o}{T}\right) = -\theta_{max}\frac{2\pi}{T}\sin\left(2\pi\frac{t_o}{T} + \Phi\right)$$

Solving for the constant, θ_{max}

$$\theta_{max} = \left(\frac{Fr}{k}\right) \frac{\sin (2\pi t_o/T)}{\sin\left[\tan^{-1}\left(\frac{\sin 2\pi t_o/T}{1 - \cos 2\pi t_o/T}\right)\right]}$$

This quantity is equal to the maximum angular displacement of the platform. It can be expressed as a ratio of the displacement that would result from an instantaneous thrust pulse of the same total impulse by using equations (10) and (11).

$$\frac{\theta_{max}}{\theta_{max\ impulse}} = \frac{F t_o}{2\pi t_o/T\, I_t} \frac{\sin (2\pi t_o/T)}{\sin\left[\tan^{-1}\left(\frac{\sin 2\pi t_o/T}{1 - \cos 2\pi t_o/T}\right)\right]}$$

but if, $F t_o = I_t$

$$\frac{\theta_{max}}{\theta_{max\ impulse}} = \frac{\sin (2\pi t_o/T)}{(2\pi t_o/T) \sin\left[\tan^{-1}\left(\frac{\sin 2\pi t_o/T}{1 - \cos 2\pi t_o/T}\right)\right]} \tag{12}$$

This quantity may be considered as a correction factor to be applied to displacement readings so that all readings are equivalent and correspond to the value that would be obtained with an instantaneous impulse. It is applicable for series durations up to one-half of the natural period of the pendulum. For short durations, the factor may be approximated by the simpler relation,

$$\frac{\theta_{max}}{\theta_{max\ impulse}} = 1 - \frac{\pi^2 (t_o/T)^2}{6} \tag{13}$$

For series durations greater than half of the natural period, the maximum deflection is very close to twice the static deflection that would occur with a uniform force of equal total impulse.

$$\theta_{max} = \frac{2Fr}{k}$$

and

$$\frac{\theta_{max}}{\theta_{max\ impulse}} = \frac{1}{\pi (t_o/T)} \tag{14}$$

This forms a hyperbolic curve that fairs into the relation given by equation (12). It is a useful relation when it is desired to find the average impulse associated with a long series of pulses. If the duration exceeds half of the period, there is no need to determine the time ratio and to find a correction factor. The average impulse can be obtained for this case by combining equations (10) and (14)

$$\text{total } I_t = \frac{\pi\sqrt{Ik}}{r} \frac{t_o}{T} \theta_{max}$$

at the end of the series of pulses, $n = ft_o$

$$\text{single pulse } I_t = \frac{\text{total } I_t}{n} = \frac{\pi\sqrt{Ik}}{rfT}\,\theta_{max}$$

$$\text{single pulse } I_t = \frac{k}{2rf}\,\theta_{max} \tag{15}$$

which is independent of the duration of the series and of the moment of inertia of the platform. However, a knowledge of the platform spring constant is required. The correction factor, which is given by equations (12) and (14), is plotted in inverse form in Figure 22.

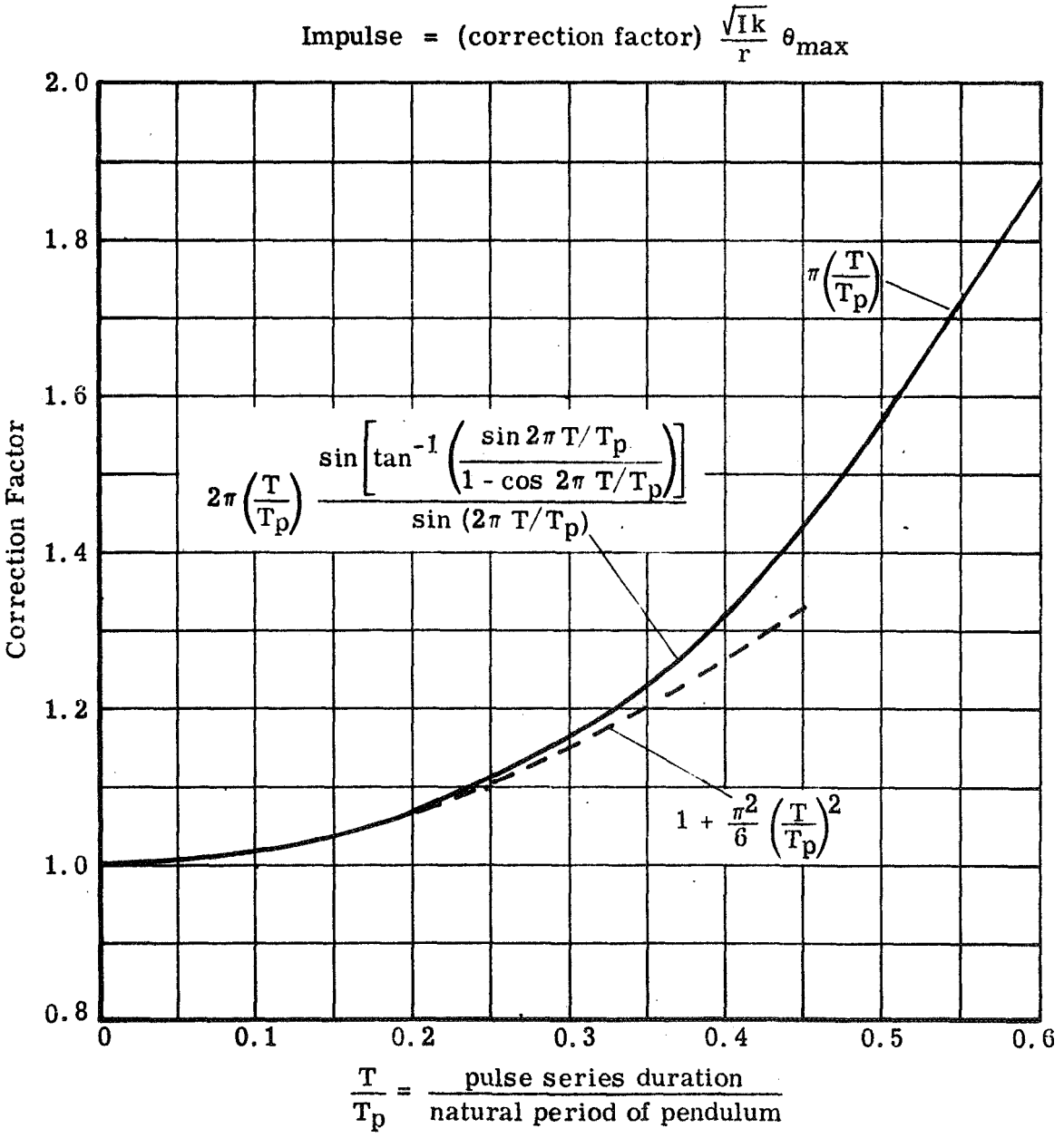

Figure 22. Correction Factor to be Applied to the Deflection of a Torsional Ballistic Pendulum when a Series of Pulses are Applied

3.4 Secondary Motion of the Platform

A source of error that has not been discussed is that caused by other oscillatory modes of the platform. The application of an impulse will start the platform swinging as a pendulum as well as rotating in torsion. Generally, the more sensitive the device is in torsion, the smaller the error will be. For the planned configuration, the displacement due to swinging is always less than two percent of the displacement due to rotation (and in many operating conditions much less). The swinging frequency will be between one and two orders of magnitude higher than the torsional frequency making it probable that the higher frequency signal can be identified and allowed for. Swinging could be limited by using a pair of thrusters or by restraining the movement of the platform to rotation alone. The latter approach would introduce other difficulties and would probably require that the base be accurately leveled (remotely) to allow for distortion of the vacuum chamber. This added complication is not believed to be justified at present.

Tests with a model torsional pendulum (described in the next section) have shown that another type of secondary motion can be of some importance. This is a rotational movement about the longitudinal axis of the beam due to the fact that the impulse is not applied at the center of percussion. This effect could be avoided by mounting the thruster at a vertical position in line with the center of percussion (determined with respect to the pivot point of the pendulum). For the model pendulum configuration this would be about 0.23 inch below the center of gravity of the beam. However, since the center of gravity of all of the equipment mounted on the beam would be laborious to determine, a better approach might be one that makes use of the fact that the center of percussion for a pendulum occurs at a distance below the pivot axis equal to the effective length of the pendulum. This distance is readily found by measuring the period of the pendulum and using the expression;

$$\ell_{\text{effective}} = \frac{T_s^2 g}{4\pi^2}$$

The measured period is 2.32 seconds which gives an effective length of 52.63 inches and locates the center of percussion 1.76 inches below the top of the bus bars that connect the capacitors. There is a difficulty involved in using this approach for the model torsional pendulum. The torsional member is a thin strip of steel which must bend in the edgewise direction as the pendulum swings. The member is very limber in torsion, but is stiff enough in bending that the location of the effective pivot axis in swinging is uncertain. The location of the center of percussion should be lower than given by the above figures to allow for this stiffening effect. If it is considered desirable to locate the center of percussion for the final design, it would be advantageous to provide a mount at the top of the torsion member that provides a definite pivot axis location for the swinging mode.

If it is impractical to locate the thruster at the same height as the center of percussion, the effect of the secondary motion can be minimized by locating the scale for measuring angular deflection at that height. In either case, however, the swinging action referred to earlier would not be eliminated. It may be desirable to devise a measuring system that is sensitive only to rotary motion. This could be done by using a pair of displacement transducers on opposite sides of the pivot axis arranged so that their signals add for a rotary displacement and cancel for a swinging movement (as suggested in Reference 15). Alternately, if the reading is taken visually, a mirror mounted on the beam could be used to deflect an optical path.

3.5 Experience With a Working Thrust Stand Model

Figure 23 shows a torsional ballistic pendulum that was constructed to determine operating characteristics and gain experience with this type of instrument. The construction used is not suitable for installation on a vacuum chamber, but a number of useful tests can be performed in normal ambient air.

The beam is supported from above its center of gravity by a thin vertical strip of steel that provides a low torsional spring constant. The arrangement permits the torsional member to be easily adjusted or modified. The thruster is at one end of the beam (Figure 24), and a graduated scale for measuring the maximum displacement is at the other end (Figure 25). The beam supports the complete engine system including the capacitor bank and the circuit for triggering the arc discharge. As a consequence, the only connecting leads required are those for charging the capacitors and controlling the triggering circuit, and these are provided by a loop of flexible cable connecting to the underside of the beam. A plywood enclosure surrounds the instrument and reduces the effect of air current on the reading. A latch for holding the beam in its neutral position until a pulse is to be applied is provided at the end of the beam as shown in Figure 25. It can be adjusted, engaged, and released from outside of the enclosure. A mechanical latch was chosen in preference to a liquid or electromagnetic damper because it appears to be easier to design a mechanical device that will be free of interaction effects during the pulse and can be released without disturbing the beam. The moving part of the latch is mounted on a stationary base and fits into a slot on the beam which provides a small clearance even with the latch fully engaged. When the device is engaged, the sides of the slot bounce off the latch repeatedly until the energy due to movement of the beam is dissipated. The latch position is adjusted with a threaded screw arrangement so that it is centered in the slot when the beam comes to rest. The latch can then be released without disturbing the beam. When the thruster is operated, the action of the arc expells air and vaporized material which produces a thrust pulse for checking out the performance of the instrument.

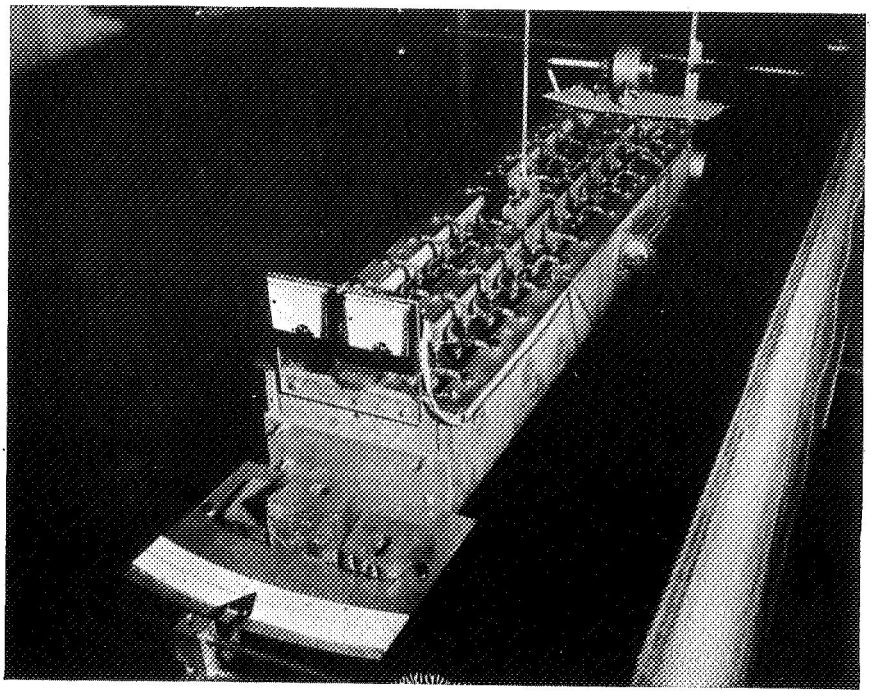

Figure 23. Working Model of the Torsional Ballistic Pendulum

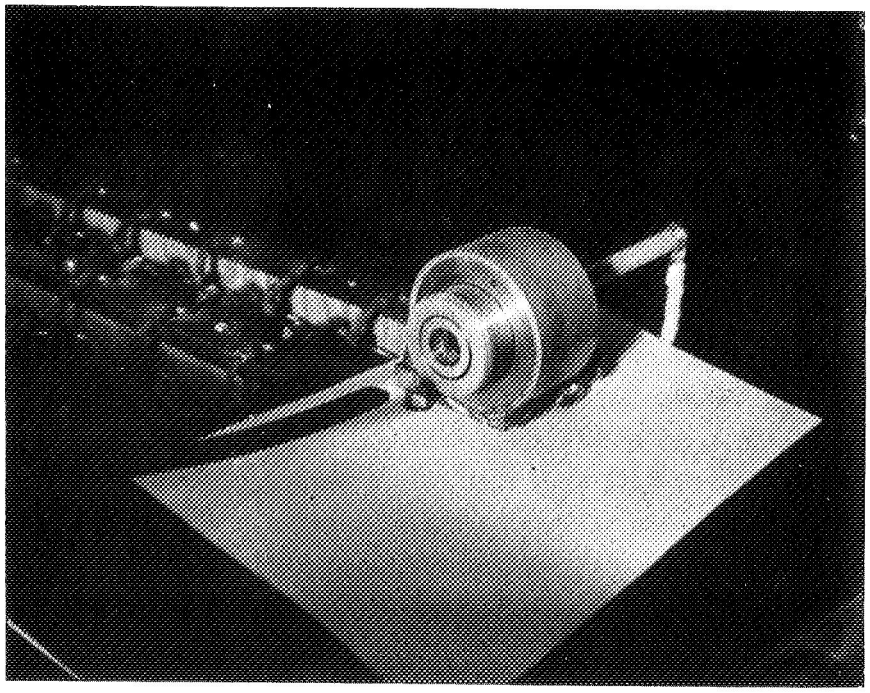

Figure 24. Thruster Mounted on the Experimental Thrust Stand

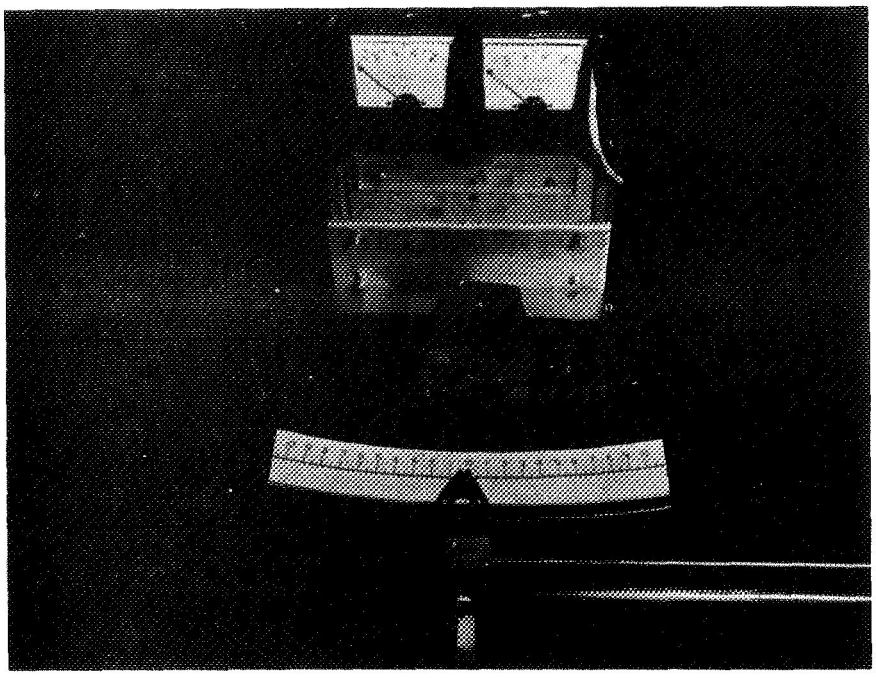

Figure 25. Graduated Scale and Latch of the Working Thrust Stand Model

3.6 Thruster Tests in Air

To check performance of the torsional pendulum with a thruster in operation, measurements were made with the thruster pulsed in air. The instrument appeared to perform properly, and no unusual or unexpected behavior was noted. Since the effective propellant mass cannot be estimated, overall performance cannot be calculated for this case. However, a beam deflection of 4.5 degrees was noted for a single pulse with a 28,800 microfarad condenser bank charged to an initial value of 450 volts. Using the calibration constant found as described in the Appendix, the impulse for this case is found to be 6380 dyne seconds. Figure 26 shows efficiency versus specific impulse for a range of assumed values for the propellant mass. The efficiency shown includes circuit losses as well as thruster losses. There are about 6.73 milligrams of air contained in the arc chamber initially. If we neglect vaporized solids and entrained ambient gas and use this value for the propellant mass, we obtain a specific impulse of 970 seconds with an overall efficiency of 0.208.

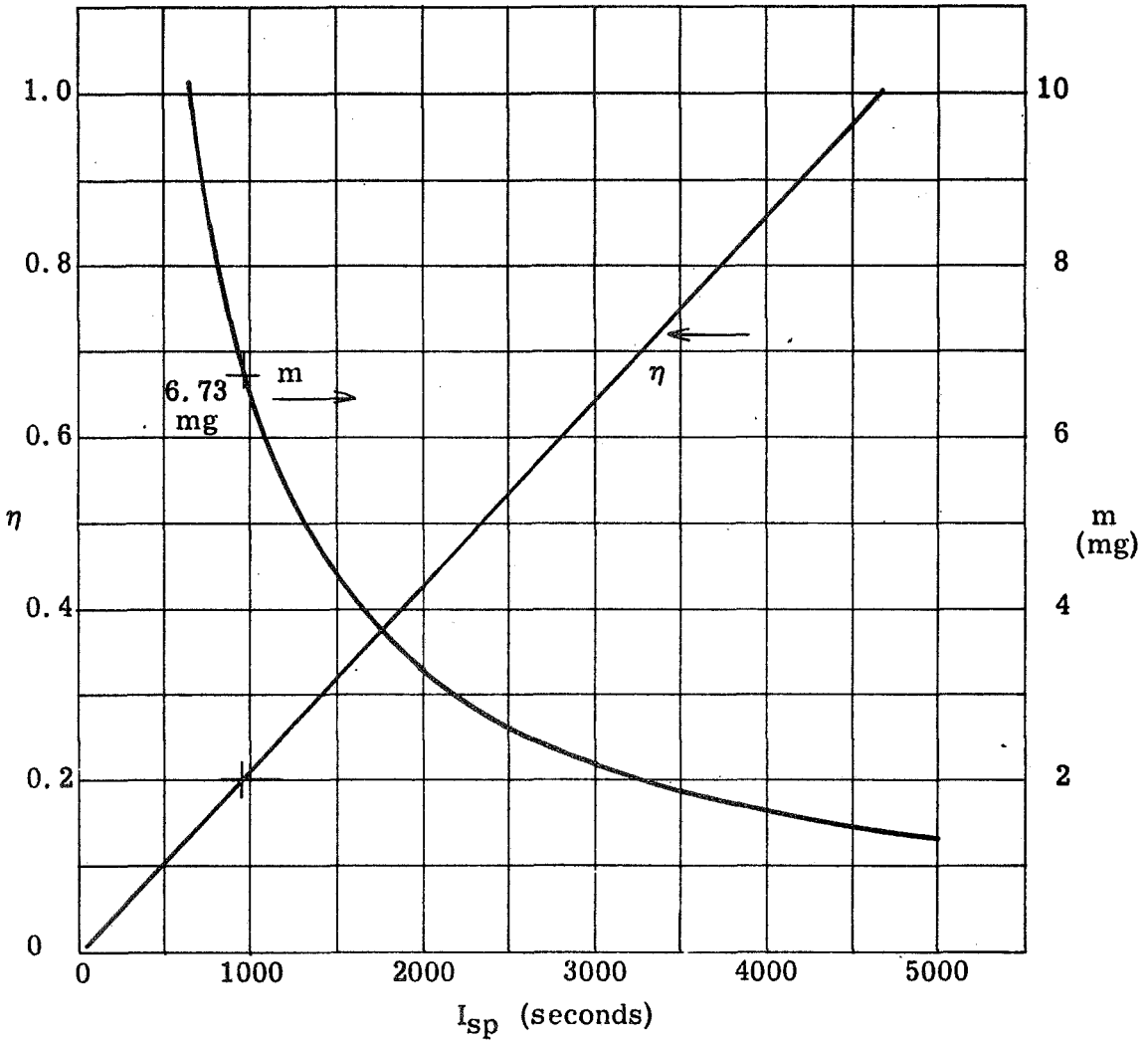

Figure 26. Possible Performance Figures for the Thruster Pulsed in Air

3.7 An Instrument for Use in the Vacuum Chamber

The experience gained with the working thrust stand model is being applied to the construction of an instrument that will be suitable for use in the vacuum chamber. Figure 27 shows the beam partially assembled. A pressurized gas tight enclosure houses the pulse generating circuit and prevents excessive evaporation of the electrolyte in the capacitors. The arrangement shown can accommodate six rows of ten capacitors each to provide a total capacitance as high as 60,000 microfarads. Subsequently, space will be provided for stepped increases in capacity to a maximum of 200,000 microfarads. The assembly will be suspended by a torsional member from the circular yoke which surrounds the enclosure.

The thruster is mounted on one of the end plates of the enclosure and is held in place by three socket head machine screws. When these screws are tightened, three electrical contacts are made in the thruster mounting base to provide current for the arc and for the arc starting circuit. Removal of the screws leaves the thruster free for removal from the thrust stand. A system has been devised for loosening the three screws, removing the thruster from the thrust stand, and withdrawing the thruster from the vacuum chamber through a valved port without releasing the vacuum in the test chamber. The hardware to accomplish this is shown in Figures 28 through 30. Figure 28 shows the probe that can be introduced into the test chamber through the valved port previously described (see Figure 21). The probe is provided with four manipulating rods which pass through it lengthwise. The rods can be rotated and moved axially through "O" ring seals. Three of the rods have hexagonal ends arranged for wrenching the socket head screws, while the fourth (center) rod has a threaded end which screws into the thruster base and holds the thruster on the probe. Figure 29 shows the thruster mounted on the end of the probe ready to be introduced into the chamber, while Figure 30 shows the opposite end of the probe with the manipulating handles visible.

The importance of being able to easily remove the thruster without losing vacuum is evident when we consider that the propellant for most of the tests is to be provided by vaporization of materials contained as an integral part of the thruster. Information on the rate of propellant expenditure and on erosion patterns on the arc chamber parts is obtained only when the thruster is removed for examination and weighing. The thruster must therefore be removed before and after each test point for which overall performance is obtained. Since it can take many hours to thoroughly evacuate and outgas the large insulated test chamber, the loss of vacuum following each test point would put an intolerable limit on the amount of data that could be obtained. Furthermore, one of the goals of the program is to determine performance with ambient gas effects minimized, which requires that the best possible vacuum be maintained at all times.

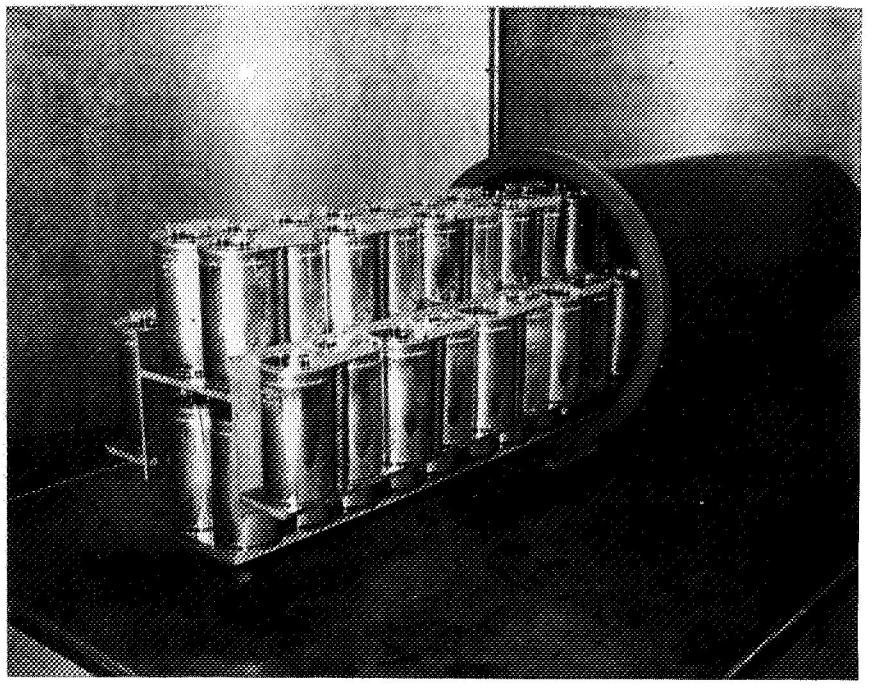

Figure 27. Torsional Ballistic Pendulum for Use in the Vacuum Chamber

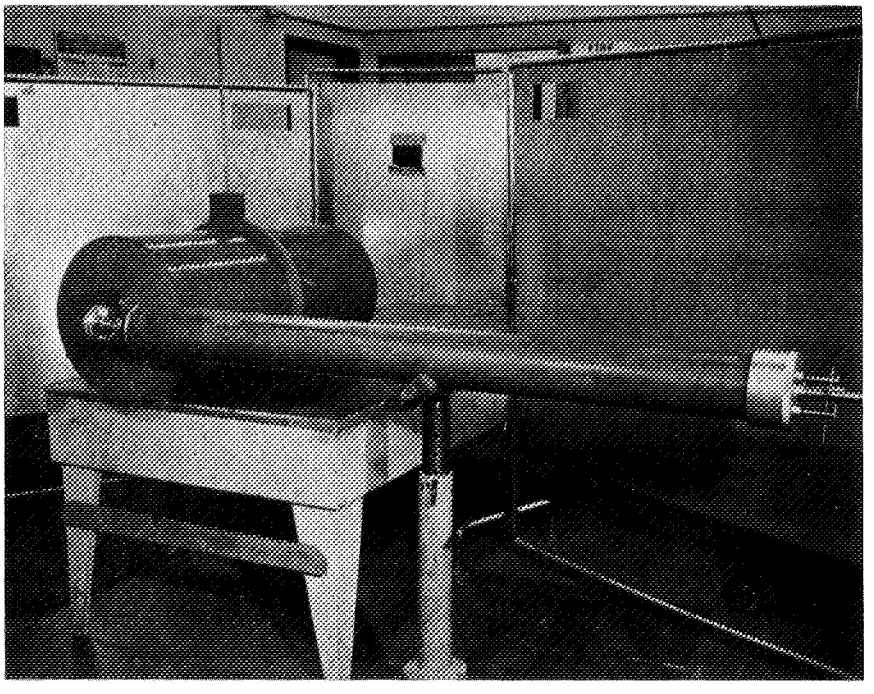

Figure 28. Manipulating Probe for Installing the Thruster Without Releasing Vacuum

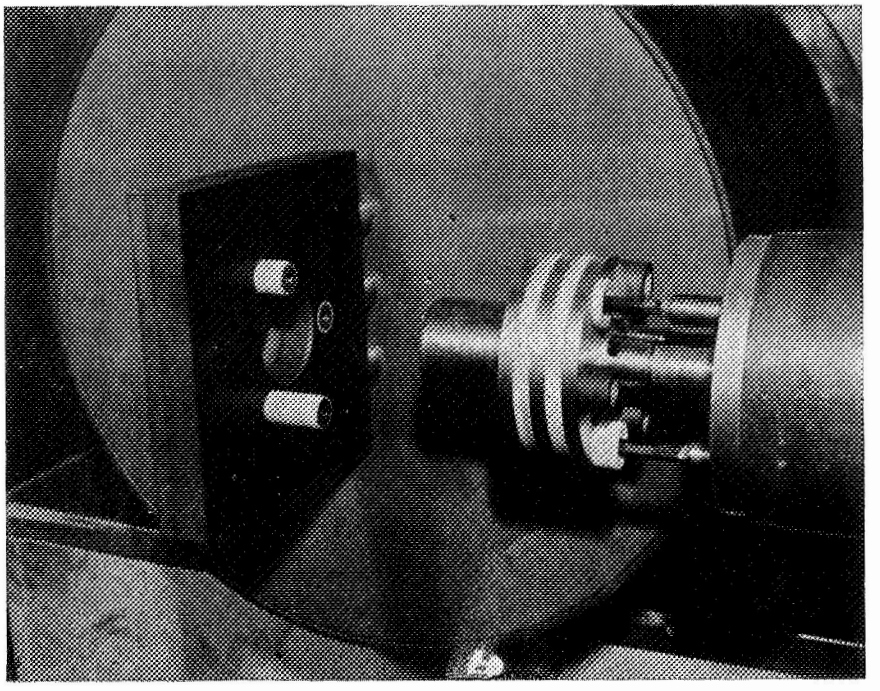

Figure 29. Thruster Attached to the Manipulating Probe

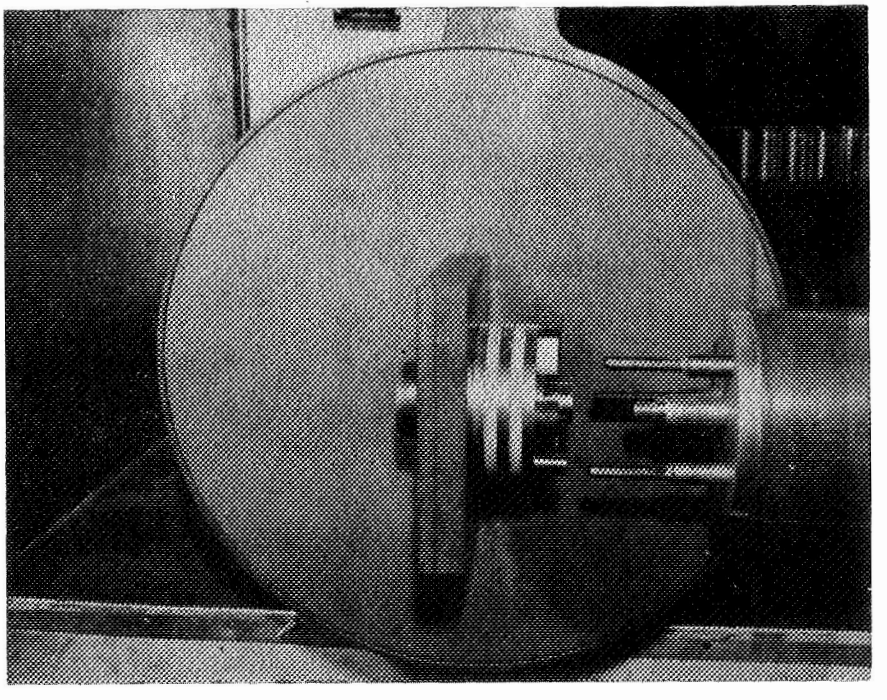

Figure 30. Handles for Mounting or Releasing the Thruster in the Vacuum Chamber

3.8 Spectroscopic Observations of the Plume

Spectrographs of the plume have been made using a Bausch and Lomb 1.5-meter grating spectrograph. The instrument has been adapted for this purpose by adding a fixture at the focal plane for mounting a 4 by 5 Polaroid film holder (Figure 31). The entire field can be photographed by shifting the film holder position in three horizontal steps. Polaroid film is used so that the Polaroid Type 57 film with a speed of 3000 a.s.a. may be utilized. Even with the high film speed, it is necessary to expose the film during 10 to 100 repetitive pulses with a slit opening between 10 and 60 microns to get an adequate exposure. A quartz lens system has been provided to permit lines in the ultraviolet range to be detected. However, a Pyrex window is still being used in the vacuum chamber which at present limits observations to wavelengths above 2500 angstroms.

Another modification involves the addition of a rotatable mounting frame with a bearing axis that coincides with the center of the incoming light path. By rotating the instrument through 90 degrees as shown in Figure 32, the slit can be made either horizontal or vertical. Photographs with the slit vertical give an indication of how the composition of the gas in the plume varies with radius, while photographs with the slit horizontal show how the composition of the gas varies with axial position in the plume. Changes in the strength of spectral lines along their length are used in determining these variations.

Figure 33 shows spectrographs obtained with several different materials used for the electrodes. These include aluminum, copper, molybdenum, tungsten, and graphite. As expected, there is a change in the lines when the electrode material is changed. However, some lines persist regardless of the electrode material showing that the plume contains significant quantities of other materials besides electrode vapor. The photographs are still being analyzed. This result suggests that spectrographs be taken with other materials substituted for the insulator in the thruster and with various gases substituted for the ambient gas in the vacuum chamber to establish the source of the remaining lines.

There is also interest in determining how the composition of the plume varies after a pulse is initiated, as this would give an indication of how rapidly various components of the thruster start to vaporize. Since the present spectrograph is a rather slow instrument, this data could only be obtained by using a high speed shutter synchronized with the repeating pulses or by rapidly moving the image with respect to the film (as is done in time resolved spectrographs) in a manner that repeats for a long series of pulses. The use of a faster instrument with a more efficient optical system is also being considered as this might, in the long run, result in a saving in both time and cost.

Spectrographs obtained using repeated exposures during successive pulses show that the lines remain relatively sharp and that repeatable results are obtained using this technique. This implies that the variation of the spectrograph with time during a pulse is also

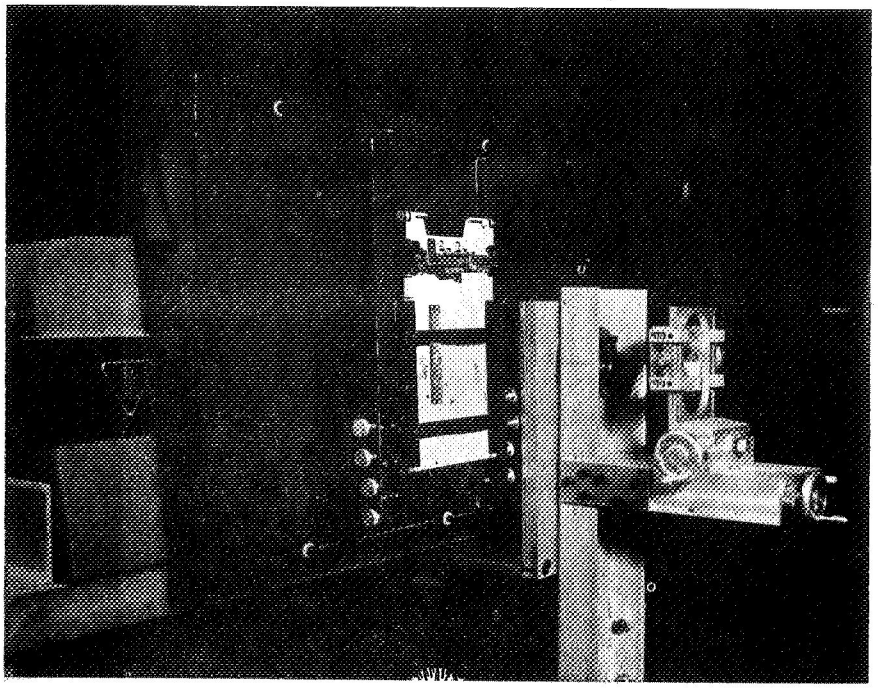

Figure 31. Film Holder Fixture for the Spectrograph

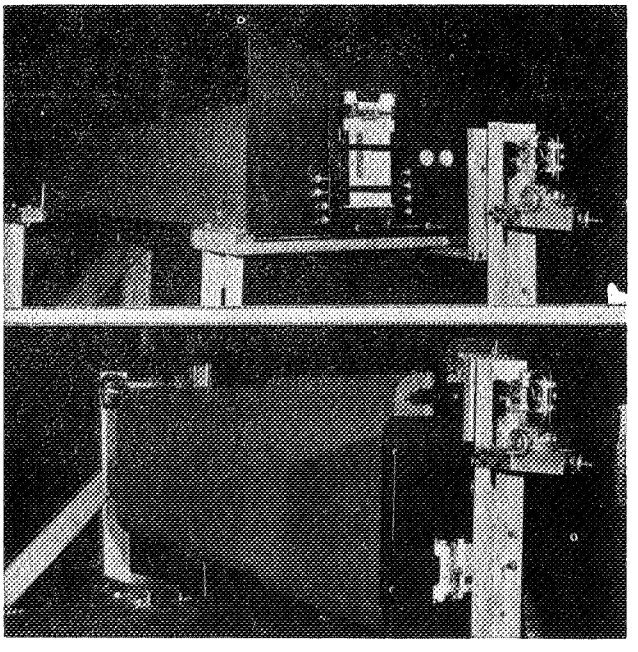

Figure 32. Arrangement for Rotating the Spectrograph Through 90°

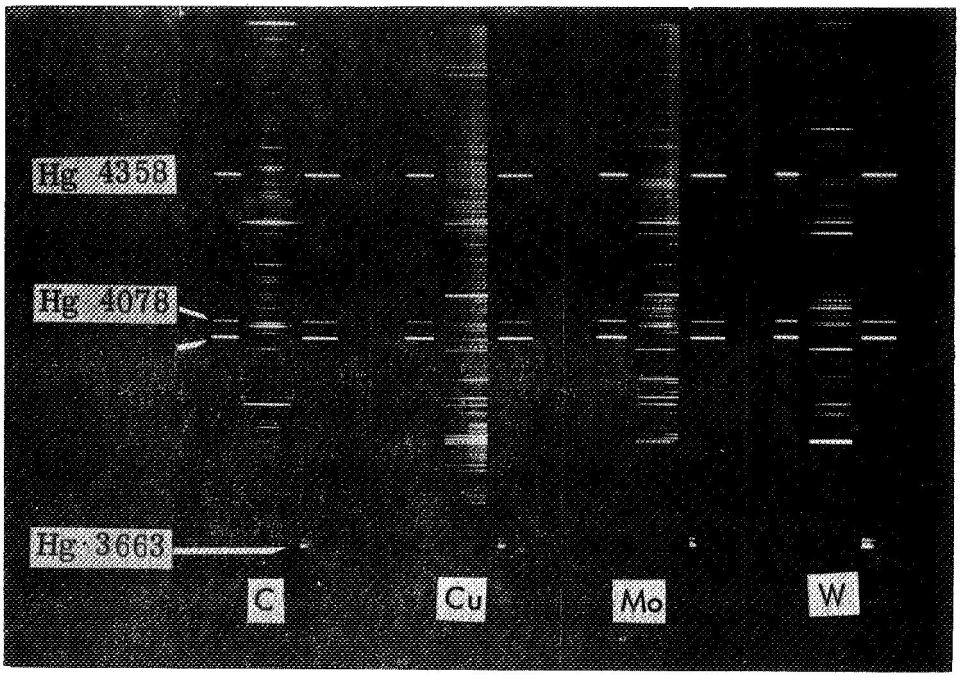

Figure 33. Spectrographs of the Plume

repeatable. It is fortunate that good results can be obtained with the instrument used in this way because the technique permits a detailed examination to be made of the pulse with location and time as variables. Lines that would be undetectable with other techniques can be photographed using a properly selected series of exposures.

4.0 CONCLUSIONS

The major results of the work described in this report are listed below.

1. It has been demonstrated that MPD thrusters can be operated in the quasi-steady mode using electrode and insulator vapor for the propellant. Initial measurements suggest that the performance is in an attractive range, but a final evaluation must be delayed until the thrust stand is put in operation.

2. A constant current discharge of reasonable duration can be obtained using a pulse generating network of electrolytic capacitors. It has been shown that the adverse effect of the high resistance of this type of capacitor can be overcome by the proper design of the network, to the extent that useful test programs can be performed.

3. There is evidence that thermal stresses are too high in some components of the thruster during pulsed operation. This is shown by initial transient heat transfer calculations and confirmed by observed distortion in the electrodes. The solid particles that are observed in the jet are also believed to result from high thermal stresses in some cases. More refined transient heat transfer studies are needed to point out design changes that will reduce or eliminate this cause of erosion.

4. It appears to be feasible to control the specific impulse within a reasonable range by a proper choice of propellant and of electrode geometry. More refined transient heat transfer studies are again needed to assess propellant vaporization rates with different propellants and different arc chamber designs.

5. The ability to accurately measure total impulse during a thrust pulse of the order of one millisecond duration has been demonstrated using a torsional ballistic pendulum. It should now be possible to determine the overall performance of quasi-steady MPD thrusters.

6. A spectrograph has been used for identifying elements in the plume, and results show that the jet includes significant quantities of other materials than electrode vapors. Further work is required to identify the source of this material. It is believed that more refined techniques and equipment will permit an evaluation of the relative concentration of elements in the jet as a function of position in the plume and time elapsed from initiation of a pulse.

REFERENCES

1. Clark, K. E. and Jahn, R. G., "Quasi-Steady Plasma Acceleration," AIAA Paper 69-267 (March 1969), to be published, AIAA Journal, February 1970.

2. Wilbur, P. J. and Jahn, R. G., "Energy Transfer From a Pulse Network to a Propagating Current Sheet," AIAA Paper 69-113 (January 1969), AIAA Journal, Vol. 8, No. 1 (January 1970) pp. 144-149.

3. Black, N. A., "Dynamics of a Pinch Discharge Driven by a High-current Pulse-forming Network," Ph. D. Thesis, Princeton University (April 1966).

4. Guman, W. J. and Nathanson, D. M., "Pulsed Plasma Micro-thruster Propulsion System for Synchronous Orbit Satellite," AIAA Paper 69-298 (March 1969).

5. Hayworth, B. R., "Energy Storage Capacitors: An Experimental and Theoretical Investigation of Their Properties," M. S. Thesis, San Diego State College (June 1964).

6. Gorowitz, B., Gloersen, P. and Karras, T., "Study of Parametric Performance of a Two-stage Repetitively Pulsed Plasma Engine (REPPAC)," G. E. Summary Report 214-220, NASA CR-54846, General Electric Missile and Space Division, Philadelphia, Pa. (March 1966).

7. Black, N. A. and Jahn, R. G., AIAA Journal, Vol. 3, No. 6 (June 1965) pp. 1209-1210.

8. Gilmour, Jr., A. S., Clark, Jr., R. J. and Veron, H., "Pulsed Vacuum Arc Micro-thrusters," AIAA Paper 67-737 (September 1967).

9. LaRocca, A. V. and Perkins, G. S., "Development of Solid Propellant Electric Thrustor Systems for Attitude Control and Station Keeping of Spacecraft," AIAA Paper 67-661 (September 1967).

10. Ducati, A. C. et al., "Recent Progress in High Specific Impulse Thermo-ionic Acceleration," AIAA Paper 65-95 (January 1965).

11. Schneider, P. J., Temperature Response Charts, John Wiley and Sons, Inc. (1963).

12. Ducati, A. C., Jahn, R. G., Muehlberger, E. and Treat, R. P., "Exploratory Electromagnetic Thruster Research," Annual Report TR 117-1513, NASA CR-62047, Giannini Scientific Corporation, Santa Ana, California (February 1968).

13. Jahn, R. G., Clark, K. E., Oberth, R. C. and Turchi, P. J., "Acceleration Pattern in Quasi-steady MPD Arcs," AIAA Aerospace Sciences Meeting, New York, N. Y. (January 1970).

14. Jahn, R. G., Physics of Electric Propulsion, McGraw-Hill Book Company, New York (1968).

15. LaRocca, A. V., Malherbe, P. and Ferrara, J., "Microthrust and Impulse Measurement Techniques for Electrical Thrusters," AIAA Paper No. 68-578 (June 1968).

APPENDIX
CALIBRATION OF THE THRUST STAND

The sensitivity of the instrument depends on the torsional spring constant and the moment of inertia of the beam. A calibration can therefore be made by determining these two quantities as well as by measuring the response to a known impulse. It follows that there are several satisfactory methods for performing a calibration.

1. Calibration Using a Steel Ball Rolling Down a Tube

In one of three calibration systems now in use, a known impulse is applied by allowing a hardened steel ball to roll down an inclined quartz glass tube arranged so that the ball strikes a vertical plate attached to the beam at the same radius as the thruster. The use of a quartz tube and a hardened steel ball result in negligible energy loss as the ball rolls down the tube. The horizontal component of the velocity of the ball may therefore be expressed;

$$Vh = \sqrt{2gh\left(\frac{1}{1+\left(\frac{2}{\sqrt{10}}\right)^2}\right)}\cos\alpha$$

where the factor $2/\sqrt{10}$ is the ratio of the radius of gyration to the outer radius of a solid sphere, and the factor in parenthesis is the fraction of the total kinetic energy (translational and rotational) that appears in translational form. The impulse applied to the beam is equal to the change in momentum experienced by the ball;

$$\text{impulse} = m\,Vh\,(1+e)$$

where e is the coefficient of restitution for the impact between the ball and the plate. In a sample calibration, a tube with a vertical drop (h) of 7.68 inches and an angle of inclination (α) of 19.2 degrees was used. The corresponding horizontal component of velocity is 64.0 inches per second. The coefficient of restitution (e) was estimated to be 0.800 by measuring the height of bounce with the plate horizontal. For a mass (m) of 8.4 grams, the corresponding impulse is 0.0215 pound seconds. The measured displacement for the case was 9 millimeters, giving

$$\text{calibration factor} = 0.00239\ \frac{\text{lb sec}}{\text{mm}}$$

with the existing capacitor bank, an impulse of 0.02 lb sec might be expected, resulting in a deflection of 8.4 mm for a single pulse. This displacement can be measured with sufficient accuracy.

2. Calibration Using a Swinging Steel Ball

In the second method, a known impulse is applied by allowing a swinging steel

ball to strike a vertical plate attached to the beam at the same radius as the thruster. The ball is suspended by a thread located so that the ball comes to rest nearly touching a vertical copper plate mounted on the thruster (see Figure 34). The thread attachment point can be adjusted for locating the neutral position of the ball and for accommodating different swinging arm lengths. The ball is drawn back to a position determined by a scale located as shown in Figure 35 and allowed to swing against the plate. The coefficient of restitution is fairly low for the impact between the ball and the copper plate, so the maximum scale reading for the backswing is also measured. We will now derive the expressions needed for calculating the impulse from the two scale readings. Referring to Figure 35, the maximum height (h) to which the ball is raised is given by;

$$h = r - \sqrt{r^2 - s^2} = r\left[1 - \sqrt{1 - \frac{s^2}{r^2}}\right] \tag{16}$$

where

$$s = s' \frac{r}{r'} = s' \frac{r}{\sqrt{(r-b)^2 + s'^2}} \tag{17}$$

and the potential energy of the ball and thread is given by;

$$\text{potential energy} = hg\left[m_{ball} + \left(\frac{1 - D/2r}{2}\right) m_{thread}\right]$$

The kinetic energy of the ball and the thread just before impact is now written

$$KE = \frac{\omega^2}{2}\left(I_{ball} + I_{thread}\right)$$

$$= \frac{1}{2}\left(\frac{V}{r}\right)^2\left[m_{ball}\left(r^2 + \left(\frac{D}{\sqrt{10}}\right)^2\right) + m_{thread}\left(\frac{r - D/2}{\sqrt{3}}\right)^2\right]$$

$$= \frac{V^2}{2}\left[m_{ball}\left(1 + \frac{(D/r)^2}{10}\right) + m_{thread}\frac{(1 - D/2r)^2}{3}\right]$$

The velocity of the ball just before impact may be found by equating the initial potential energy to the final kinetic energy;

$$V = \sqrt{2gh\left(\frac{1 + \frac{1 - D/2r}{2}\frac{m_{thread}}{m_{ball}}}{1 + \frac{1}{10}\frac{D^2}{r^2} + \frac{(1 - D/2r)^2}{3}\frac{m_{thread}}{m_{ball}}}\right)} \tag{18}$$

where the factor in parentheses corrects for the mass of the thread and the rotational energy of the ball. The impulse is equal to the momentum change, and is given by;

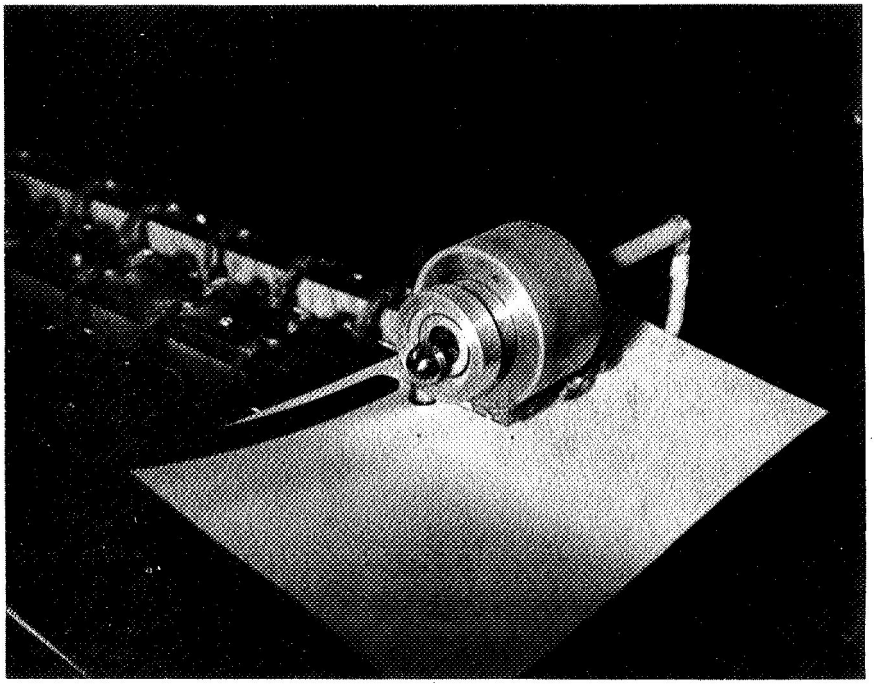

Figure 34. Swinging Steel Ball Used for Calibration

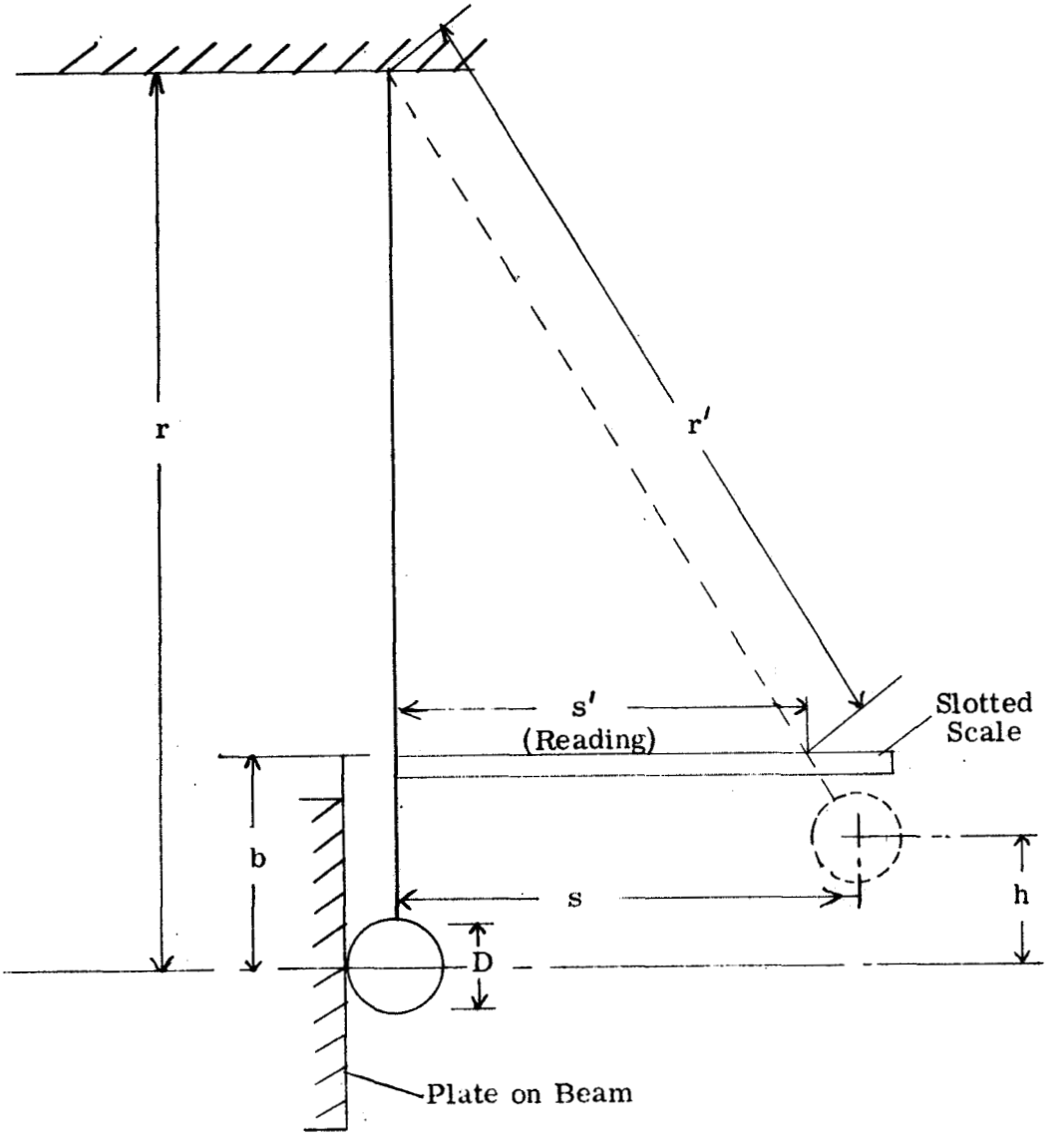

Figure 35. Configuration of the Swinging Ball Used for Calibration of the Torsional Pendulum

$$\text{impulse} = \frac{1}{r}\,(I_{ball} + I_{thread})\,(\omega_1 - \omega_2)$$

$$= \frac{1}{r}\left[m_{ball}\left(r^2 + \left(\frac{D}{\sqrt{10}}\right)^2\right) + m_{thread}\left(\frac{r - D/2}{\sqrt{3}}\right)^2\right]\left(\frac{V_1 - V_2}{r}\right)$$

$$= m_{ball}\left[1 + \frac{1}{10}\,\frac{D^2}{r^2} + \frac{(1 - D/2r)^2}{3}\,\frac{m_{thread}}{m_{ball}}\right](V_1 - V_2)$$

Substituting equation (18)

$$\text{impulse} = m_{ball}\sqrt{2g\left[1 + \left(\frac{1 - D/2r}{2}\right)\frac{m_{thread}}{m_{ball}}\right]\left[1 + \frac{1}{10}\,\frac{D^2}{r^2} + \frac{(1 - D/2r)^2}{3}\,\frac{m_{thread}}{m_{ball}}\right]} \cdot (\sqrt{h_1} + \sqrt{h_2}) \qquad (19)$$

The factors in brackets correct for the mass of the thread and the rotational momentum of the ball. With the configuration used, the correction is less than one percent. When the configuration of the swinging ball and the two scale readings are known, the impulse may be calculated using equations (16), (17) and (19). Figures for the two configurations used are listed below.

	First Configuration	Second Configuration
r (inches)	88.060	24.00
b (inches)	1.103	3.87
D (inches)	0.750	0.75
m_{ball} (grams)	27.650	27.65
m_{thread} (grams)	0.624	0.17

The data taken and the calculated impulses are tabulated below. Coefficients of restitution were also calculated to see how consistent the measured value of the quantity is.

Configuration	Swinging Ball Scale Readings (inches) First	Second	θ_{max} (degrees)	Impulse (dyne sec)	Coefficient of Restitution
First	4.0	2.75	0.60	867	0.648
First	5.0	3.10	0.70	1069	0.579
First	6.0	4.00	0.85	1353	0.636
First	7.0	4.40	1.08	1562	0.603
First	8.0	4.95	1.17	1794	0.595
First	9.0	5.20	1.42	1980	0.554
First	10.0	5.70	1.50	2204	0.550
First	11.0	6.10	1.70	2411	0.536

Configuration	Swinging Ball Scale Readings (inches) First	Second	θ_{max} (degrees)	Impulse (dyne sec)	Coefficient of Restitution
Second	4.0	2.20	1.45	1771	0.497
Second	5.0	3.00	1.74	2359	0.568
Second	6.0	3.25	1.96	2756	0.515
Second	7.0	3.95	2.30	3291	0.548
Second	8.0	4.20	2.65	3668	0.515
Second	9.0	4.90	2.95	4179	0.544
Second	10.0	5.25	3.35	4564	0.532
Second	11.0	5.30	3.50	4842	0.493

These results are plotted in Figure 36 as circles for the first configuration and squares for the second configuration. The scatter is not considered unreasonable in view of the relatively coarse scale used for reading angular deflection of the beam (divisions are at one-half degree intervals for the model). The coefficient of restitution is plotted in Figure 37. The relatively large scatter shown for this value is probably due, at least in part, to the difficulty experienced in accurately reading the maximum scale reading as the ball bounces off of the plate (one inch graduations were used, and a quick reading was required to estimate the maximum swing). This explanation seems to be supported by the reduced scatter shown in Figure 38 which shows calibration points adjusted for a constant value of 0.55 for the coefficient of restitution. On the other hand, the low value of the coefficient of restitution, and the tendency of the value to be less at higher impulses suggest that the copper is being deformed slightly by the impact of the ball. It is conceivable that the ball would bounce differently depending on whether or not it strikes the same spot again. A plate of quartz or hardened steel has been substituted for the copper to assure a large and constant value for the coefficient of restitution. A more accurate value for the coefficient will then be determined by measuring the maximum deflection following a number of bounces.

3. Calibration Using a Gas Jet of Known Thrust

For small values of impulse, calibration points may be obtained using a small gas jet of known thrust force. Use is made of the fact that the thrust force produced by a gas jet is relatively constant if a uniform upstream pressure is maintained. The thrust force is found by letting the jet impinge on the pan of an analytical balance, following which the beam deflection is measured with the same jet impinging on a vertical surface located at the same radius as the thruster. The arrangement is shown in Figure 39. Gas is supplied to the calibration jet through a pressure regulator to maintain a constant thrust. The analytical balance is located beside the test stand to permit the two measurements to be made in succession with minimum change in the operating conditions. In addition, it

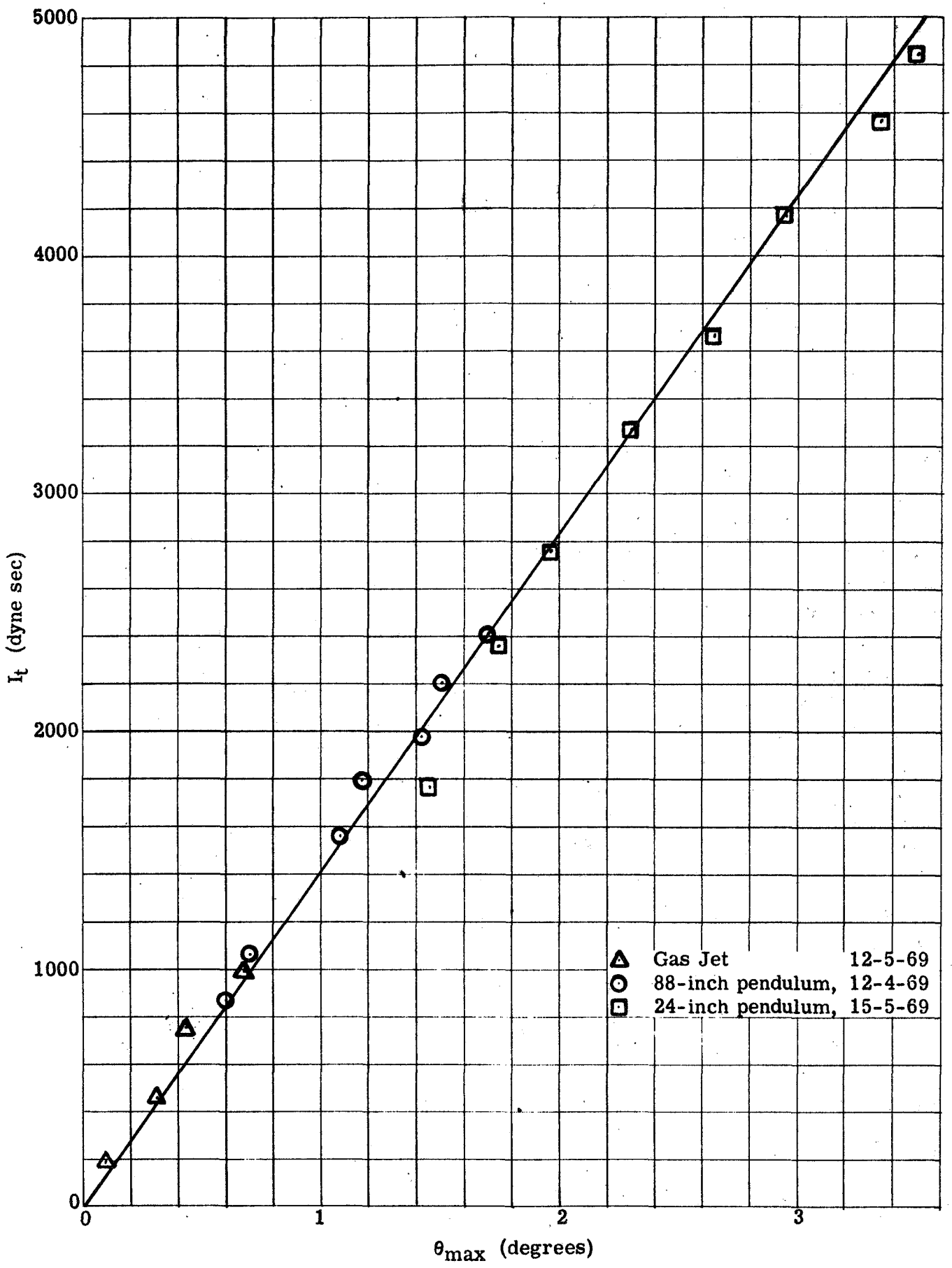

Figure 36. Calibration of the Torsional Pendulum

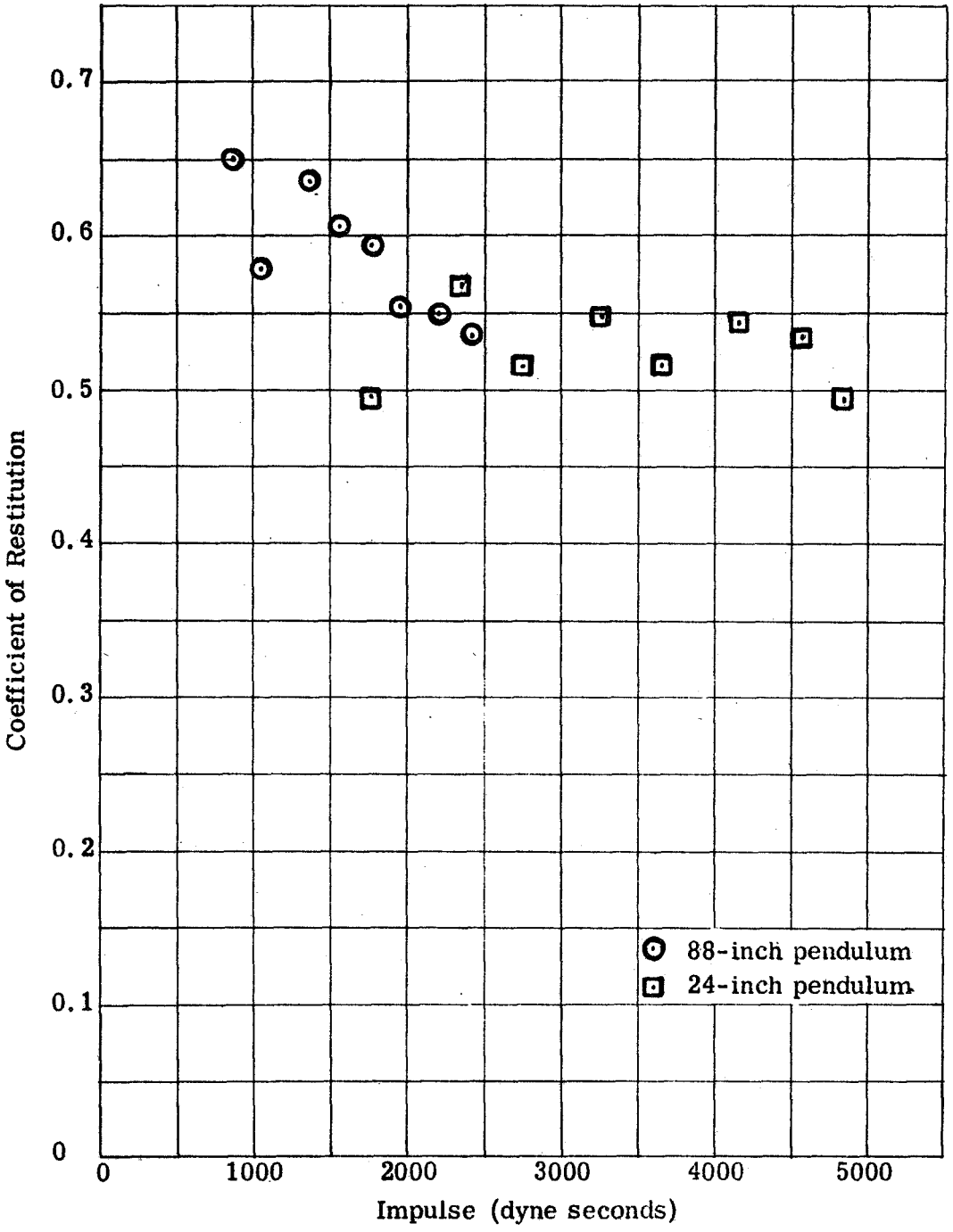

Figure 37. Measured Coefficient of Restitution for the Swinging Ball Calibration Setup

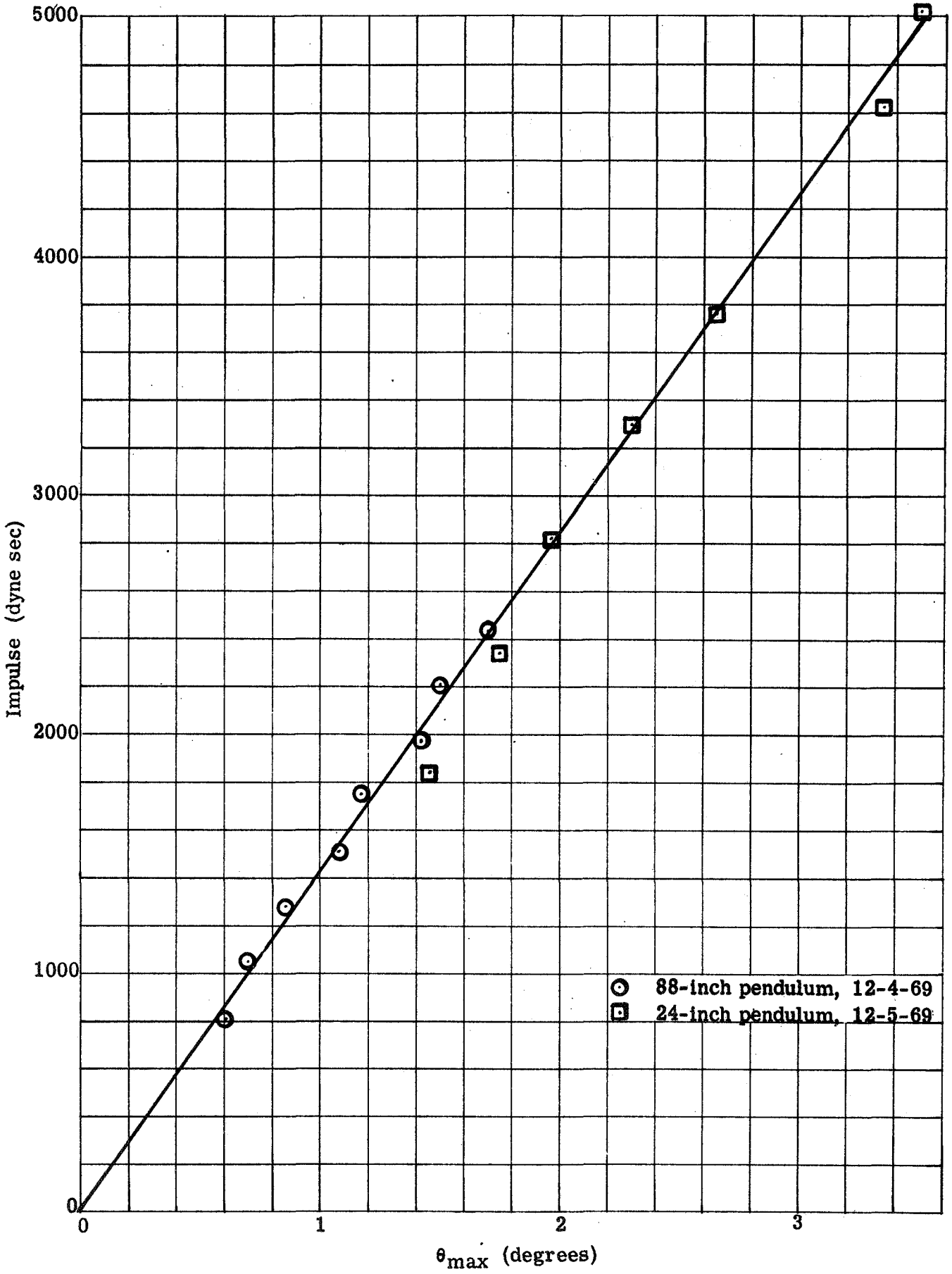

Figure 38. Calibration Points Obtained With the Swinging Ball Adjusted for a Constant Value of 0.55 for the Coefficient of Restitution

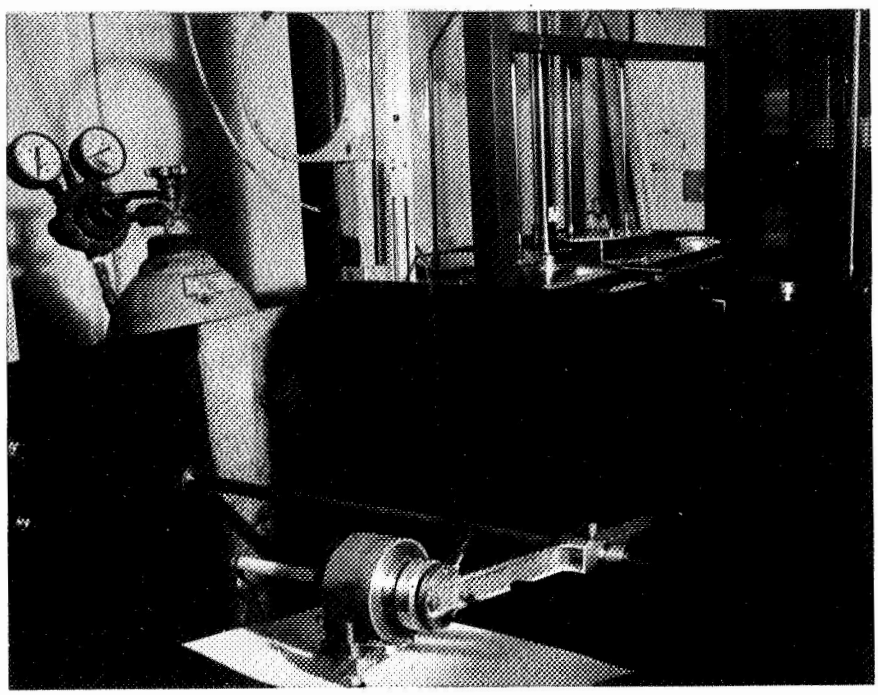

Figure 39. Arrangement for Calibration With a Gas Jet

is necessary to know the natural period of the torsional pendulum. This was found to be 137.5 seconds by timing ten cycles with a stop watch. With this information the calibration factor may be found as follows:

Using equation (10)

$$I_t = \frac{\sqrt{Ik}}{r}\,\theta_{max}$$

But the natural period of the beam is

$$T = 2\pi\sqrt{\frac{I}{k}} \quad \text{so} \quad \sqrt{I} = \frac{T}{2\pi}\sqrt{k}$$

Substituting

$$I_t = \frac{Tk}{2\pi r}\,\theta_{max}$$

The spring constant (k) is determined in effect by observing the effect of the jet on the beam. If the jet impinges on the thrust platform at the same radius (r) at which the thrust acts, and the displacement is measured at radius (R), the torsional spring constant may be written;

$$k = \frac{fr}{(x'/R)} = \frac{frR}{x'}$$

Substituting in the preceding equation,

$$I_t = \frac{TfrR}{2\pi r x'}\,\theta_{max}$$

$$\text{but} \quad \theta_{max} = \frac{x}{R}$$

So

$$I_t = \frac{Tf}{2\pi x'}\,x$$

and

$$\text{calibration factor} = \frac{Tf}{2\pi x'}$$

The impulse that corresponds to the measured angular deflection is obtained by multiplying the calibration factor by x';

$$\text{equivalent impulse} = \frac{T}{2\pi}\,f = 21.9 \text{ seconds } f$$

The data obtained is tabulated below.

Gas Pressure (inches of manometer fluid)	Jet Force (mg)	Jet Force (dynes)	Equivalent Impulse (dyne sec)	Average Torsional Pendulum Deflection (degrees) (reading)	(change)
0	0	0	0	0.06	0
1.80	9	8.8	193	0.15	0.09
3.75	21	20.6	451	0.37	0.31
5.30	35	34.4	753	0.49	0.43
7.26	46	45.1	987	0.73	0.67

This data is shown as triangular points in Figure 36. The jet calibration method has the advantage that it can be readily adapted for use in a vacuum chamber. In addition, the beam does not have to be brought to a complete rest between data points since deflection can be determined from readings at both ends of a swing, allowing a calibration curve to be obtained more rapidly. However, with the present arrangement, the maximum beam deflection permissible is limited by the fact that the jet is in a fixed location. Large beam deflections result in too large a space between the orifice and the target plate. With this condition, the impingement force may be less than the true jet thrust. For this reason, other calibration methods were used for the higher values of impulse.

4. Calibration by Measuring the Period of the Beam With and Without Added Weights

This approach allows the calibration factor to be determined without applying known external forces to the beam. The method, in effect, finds the quantities r, I and k which appear on the right hand side of equation (10).

The quantity Ik can be found by measuring the natural period with and without the addition to the platform of weights of known moment of inertia, ΔI. The natural periods can be expressed:

$$T_1 = 2\pi\sqrt{\frac{I}{k}} \quad \text{and} \quad T_2 = 2\pi\sqrt{\frac{I+\Delta I}{k}}$$

from which expressions for the two unknowns I/k and $\Delta I/k$ may be found,

$$\frac{I}{k} = \frac{T_1^2}{4\pi^2} \qquad \frac{\Delta I}{k} = \frac{T_2^2 - T_1^2}{4\pi^2} \tag{20}$$

and

$$\sqrt{Ik} = \frac{\sqrt{I/k}}{(\Delta I/k)}\,\Delta I = \frac{2\pi T_1}{T_2^2 - T_1^2}\,\Delta I$$

The expression for the sensitivity may now be written

$$\frac{\theta_{max}}{I_t} = \frac{r\,(T_2^2 - T_1^2)}{2\pi T_1 \Delta I}$$

This relation can be used for calibrating the instrument. The quantities r, T_1 and T_2 can all be measured with good accuracy, and the moment of inertia (ΔI) of the added weights can be precisely determined if the dimensions and masses of the weights are accurately known.

The data obtained for this calibration may also be used for the case with a series of pulses which is longer than half of the period of the platform. Using equation (20)

$$k = \frac{4\pi^2 \Delta I}{T_2^2 - T_1^2}$$

and substituting in equation (15) the sensitivity may be written

$$\frac{\theta_{max}}{I_t} = \frac{rf\,(T_2^2 - T_1^2)}{2\pi^2 \Delta I} \qquad (21)$$

Taking the slope of the calibration curve shown in Figure 36, the calibration constant for the experimental thrust stand was found to be 1417 dyne seconds per degree of angular deflection. With a 20,000 microfarad pulse generating circuit we might expect an impulse of about 4500 dyne seconds per pulse or an angular deflection of 3.18 degrees (a scale movement of 3.9 cm at a radius of 70 cm). This is an adequate movement for accurate measurement.

An observation made during the calibration is that a great deal of care is needed to be certain that the beam is accurately nulled and at rest before an impulse is applied. Since the natural period of the beam is more than two minutes, an initial movement of the beam that would result in a significant error for the final reading is barely perceptible. If the latch touches the beam while being released, an appreciable movement can be introduced. It was found possible to obtain repetitive data by limiting test points to those cases for which the beam remained in a sensibly fixed position for thirty seconds after release of the latch. This assures that the beam is both accurately nulled and at rest.

UNCLASSIFIED

Security Classification

DOCUMENT CONTROL DATA - R & D

(Security classification of title, body of abstract and indexing annotation must be entered when the overall report is classified)

1. ORIGINATING ACTIVITY (Corporate author)	2a. REPORT SECURITY CLASSIFICATION
Plasmadyne, a division of Geotel, Inc. 3839 South Main Street Santa Ana, California	UNCLASSIFIED
	2b. GROUP NASA CR 66923

3. REPORT TITLE

EXPLORATORY ELECTROMAGNETIC THRUSTER RESEARCH, PHASE III

4. DESCRIPTIVE NOTES (Type of report and inclusive dates)

Scientific

5. AUTHOR(S) (First name, middle initial, last name)

Adriano C. Ducati Robert G. Jahn

6. REPORT DATE	7a. TOTAL NO. OF PAGES	7b. NO. OF REFS
February 1970	60	15

8a. CONTRACT OR GRANT NO.	9a. ORIGINATOR'S REPORT NUMBER(S)
NAS 1-9297	FR-020-9297
b. PROJECT NO. L 13-73	
c.	9b. OTHER REPORT NO(S) (Any other numbers that may be assigned this report)
d.	

10. DISTRIBUTION STATEMENT

11. SUPPLEMENTARY NOTES	12. SPONSORING MILITARY ACTIVITY
	National Aeronautics and Space Adm. Langley Research Center Hampton, Virginia 23365

13. ABSTRACT

The work reported here is concerned primarily with setting up an initial engine system and with developing techniques for measuring performance of MPD arc jets operating in the quasi-steady mode. This type of operation is obtained by running the thruster at a high power level for a pulse period of the order of one millisecond; a period which is short enough to avoid the major problems associated with continuous high power operation, but long enough that steady state operating conditions appear to be attained during most of the pulse duration. The possibility exists of realizing the performance advantages of high power operation without the need for a space power system capable of continuous operation at high power levels, and without encountering the heating problems and life problems associated with continuous high power operation. In addition, operation in short pulses may permit more meaningful test results to be obtained. For example, with a pulsed thruster it is possible to thoroughly evacuate the test chamber before initiating the pulse so that actual space conditions are more closely simulated. Furthermore, there is the possibility of using certain probe measurements in the plume that would be impractical with steady operation.

Work has focused on the use of solid and liquid propellants. These materials can be attractive because of their good storability, and with some solid materials, it may be feasible to use rods or sleeves of propellant as electrodes or insulating components that are continuously renewed by feeding to offset the rate of erosion. Another possibility is that waste materials or discardable spacecraft hardware can be utilized for propellant.

DD FORM 1 NOV 65 1473

UNCLASSIFIED

Security Classification

14. KEY WORDS	LINK A		LINK B		LINK C	
	ROLE	WT	ROLE	WT	ROLE	WT
Arc Jet Environment						
Electrode Erosion						
Electrolytic Capacitors						
High Specific Impulse						
MPD Arc Jet						
MPD Test Environment						
Plasma Accelerator						
Plasma-Pulsed Accelerator						
Propulsion						
Pulse Networks						
Pulsed Propellants						
Quasi-Steady						
Thrust Balance						
Vacuum Chambers						